

EFFECTS OF SPECIMEN HEIGHT AND LOADING SPAN ON THE  
FRACTURE TOUGHNESS OF DISC TYPE ROCK SPECIMENS  
UNDER THREE POINT BENDING

A THESIS SUBMITTED TO  
THE GRADUATE SCHOOL OF NATURAL AND APPLIED  
SCIENCES  
OF  
MIDDLE EAST TECHNICAL UNIVERSITY

BY

Y. BURKAY TEZ

IN PARTIAL FULFILLMENT OF THE REQUIREMENTS  
FOR  
THE DEGREE OF MASTER OF SCIENCE  
IN  
MINING ENGINEERING

MAY 2008

Approval of the thesis:

**EFFECTS OF SPECIMEN HEIGHT AND LOADING SPAN ON THE  
FRACTURE TOUGHNESS OF DISC TYPE ROCK SPECIMENS  
UNDER THREE POINT BENDING**

submitted by **Y.BURKAY TEZ** in partial fulfillment of the requirements for the degree of **Master Degree in Mining Engineering Department, Middle East Technical University** by,

Prof. Dr. Canan Özgen \_\_\_\_\_  
Dean, Graduate School of **Natural and Applied Sciences**

Prof. Dr. Celal Karpuz \_\_\_\_\_  
Head of Department, **Mining Engineering**

Assoc. Prof. Dr. Levent Tutluoğlu \_\_\_\_\_  
Supervisor, **Mining Engineering Department., METU**

**Examining Committee Members:**

Prof. Dr. Tevfik Guyagüler \_\_\_\_\_  
Mining Engineering Dept., METU

Prof. Dr. Celal Karpuz \_\_\_\_\_  
Mining Engineering Dept., METU

Assoc. Prof. Dr. Levent Tutluoglu \_\_\_\_\_  
Mining Engineering Dept., METU

Prof. Dr. Bahtiyar Ünver \_\_\_\_\_  
Mining Engineering Dept., HU

Assist. Prof. Dr. Mehmet Ali Hindistan \_\_\_\_\_  
Mining Engineering Dept., HU

Date : \_\_\_\_\_

**I hereby declare that all information in this document has been obtained and presented in accordance with academic rules and ethical conduct. I also declare that, as required by these rules and conduct, I have fully cited and referenced all material and results that are not original to this work.**

**Name, Last name: Y. Burkay Tez**

**Signature :**

# ABSTRACT

## EFFECTS OF SPECIMEN HEIGHT AND LOADING SPAN ON THE FRACTURE TOUGHNESS OF DISC TYPE ROCK SPECIMENS UNDER THREE POINT BENDING

Tez, Y. Burkay

M.Sc., Department of Mining Engineering

Supervisor: Assoc. Prof. Dr. Levent Tutluoğlu

May 2008, 94 pages

A relatively new fracture toughness testing method called Straight Notched Disc Bending (SNDB) was used before for fracture testing of Ankara Andesite and Afyon Marble cores. In this work to investigate the applicability of the new method to other rock types. With a preliminary notch of 10 mm, straight notched disc type specimens with a diameter of 75 mm were loaded by three-point bending loads.

Investigation of effect of specimen height on the stress intensity factor and fracture toughness was carried out. Specimen heights (B) between 18 – 67 mm were tried for andesite and marble cylindrical specimens. Loading span, that is span/radius (S/R) ratio was changed between 0.6 - 0.9 for andesite specimens.

Stress intensity factor for specimens was computed with ABAQUS program. Stress intensity factor was found to increase with increasing specimen diameter for a fixed span/radius ratio. Stress intensity factor decreased with increasing specimen height.

Changing span was found to have no significant effect on fracture toughness of andesite. Fracture toughness was significantly lower for specimens with smaller

height. The suggested testing height interval for this type of specimens was between height/diameter ratios of 0.49 – 0.64. Results were compared to the results obtained by a well-known specimen geometry named semi-circular bend specimens (SCB) under three-point bending. SCB tests produced lower values for fracture toughness for both rock types.

Fracture toughness was  $0.99 \text{ MPa}\sqrt{\text{m}}$  for Ankara Andesite and  $0.70 \text{ MPa}\sqrt{\text{m}}$  for Afyon Marble.

Keywords : Stress Intensity Factor, Fracture Toughness, 3D Modelling, Ankara Andesite, Afyon Marble

# ÖZ

## ÜÇ NOKTADAN EĞİLME DİSK TİP ÖRNEKLERDE, ÖRNEK YÜKSEKLİĞİNİN VE DESTEK MESAFESİNİN ÇATLAK TOKLUĞUNA ETKİSİ

Tez, Y. Burkay

Yüksek Lisans, Maden Mühendisliği Bölümü

Tez Yöneticisi: Doç. Dr. Levent Tutluoğlu

Mayıs 2008, 94 sayfa

Yeni bir test yöntemi olan Düz Çentikli Disk Eğilmesi, Ankara Andezit karotlarının çatlak testleri için kullanılmıştır. Bu çalışmada bu yeni test yönteminin yeni kaya türlerinde, Afyon mermeri , kullanımı ve uygun olup olmadığı araştırılmıştır. Tüm test numuneleri 75 mm çapında olup 10 mm'lik çentik açılarak hazırlanmıştır.

Örnek yüksekliğinin gerilme şiddet faktörü ve çatlak tokluğu üzerindeki etkisi araştırılmıştır. Örnek yüksekliği (B) olarak 18 - 67 mm'ler arası kullanılmıştır. Destek aralığı örnek çapı ile orantılı olarak, destek aralığı/çap (S/R) andezit andezit örnekleri için 0.6 – 0.9 arasında değiştirilmiştir.

Gerilme şiddet faktörü değerleri üç boyutlu sayısal modelleme programı olan ABAQUS ile hesaplanmıştır. Gerilme şiddet faktörünün sabit destek aralığında (S/R) artan çap değeri ile arttığı bulunmuştur. Gerilme şiddet faktörünün numune yüksekliği arttıkça düştüğü saptanmıştır.

Değişen destek aralığının andezitin çatlak tokluğu üzerinde önemli bir değişim oluşturmadığı görülmüştür. Düşük yükseklikteki numunelerin düşük çatlak tokluğu

değerlerine sahip olduğu saptanmıştır. Bu tip örnekler için önerilen örnek yüksekliği yükseklik/çap oranı olarak 0.49 – 0.64 aralığında olmasıdır. Bulunan değerler iyi bilinen yarım dairesel eğilme numuneleri tekniği kullanılarak yapılan deney sonuçları ile karşılaştırılmıştır. Yarım dairesel eğilme örnekleri tekniğinin her iki kaya türü için de Düz Çentikli Disk Eğilmesi'ne göre daha düşük değerler verdiği görülmüştür.

Çatlak tokluğu değeri Ankara Andezit'i için  $0.99 \text{ MPa}\sqrt{\text{m}}$  , Afyon Mermer'i için  $0.70 \text{ MPa}\sqrt{\text{m}}$  bulunmuştur.

Anahtar Kelimeler : Gerilme Şiddeti Faktörü, Çatlak Tokluğu, 3 Boyutlu Modelleme, Ankara Andezit, Afyon Mermer

*To My Family...*

## ACKNOWLEDGEMENT

I would like to express my deep and sincere gratitude to my supervisor, Assoc. Prof. Dr. Levent Tutluoglu for his technical advices and constructive comments throughout this thesis.

I want to acknowledge to the examining committee the members, Prof. Dr. Celal Karpuz, Prof. Dr. Teyfik G yag ler, Prof. Dr. Bahtiyar  nver and Assit. Prof. Dr Mehmet Ali Hindistan for being interested in and reading this thesis.

I like to give special thanks to Gizem Sınav for her spiritual and material support and love and also my dear friend Kıvanç Het for helping me till the end of thesis with all his effort.

I would like to thank to Arman Koal, Tahsin Isıksal, Hakan Uysal for their help during laboratory work.

I want to thank to Ceyda Atlı and iğdem Alkılıgil for their help in ABAQUS, MTS tests and thesis work.

I want to thank my parents for their patience and encouragement.

At last, I would like to thank all whose direct and indirect support helped me completing my thesis in time.

# TABLE OF CONTENTS

PLAGIARISM.....	iii
ABSTRACT.....	iv
ÖZ.....	vi
DEDICATION.....	viii
ACKNOWLEDGEMENT.....	ix
TABLE OF CONTENTS.....	x
LIST OF TABLES.....	xiii
LIST OF FIGURES .....	xiv
LIST OF SYMBOLS AND ABBREVIATIONS.....	xvii
CHAPTER	
1. INTRODUCTION.....	1
1.1 General.....	1
1.2 Statement of the Problem and the Thesis Objective.....	2
1.3 Methodology.....	2
1.4 Sign Convention.....	3
1.5 Outline of the Thesis.....	4
2. FRACTURE MECHANICS.....	5
2.1 Historical Overview.....	5
2.2 Linear Elastic Fracture Mechanics.....	7
2.3 Loading Modes.....	8
2.4 Crack Tip Stress and Stress Intensity Factor.....	8
2.5 Fracture Criteria.....	13
2.6 Fracture Toughness.....	14
2.7 Elastic Plastic Fracture Mechanics .....	14
3. ROCK FRACTURE TESTING ON DISC TYPE SPECIMENS.....	15
3.1 Cracked Chevron-Notched Brazilian Disc (CCNBD) Specimens.....	15
3.2 Short Rod (SR) Method.....	17
3.3 Chevron Bend (CB) Method.....	19
3.4 Straight Notch Brazilian Discs (SNBD) Method.....	20

3.5 Straight Notch Semi-Circular Bending (SNSCB) Method.....	22
3.6 Summary of Results od Fracture Testing on Rock Cores.....	24
4. NUMERICAL MODELING FOR ESTIMATION OF STRESS INTENSITY	
FACTORS.....	25
4.1 Finite Element Program ABAQUS.....	25
4.2 ABAQUS Capabilities.....	26
4.3 ABAQUS Modules.....	27
4.3.1 Part Module.....	27
4.3.2 Property Module.....	27
4.3.3 Assembly Module.....	27
4.3.4 Step Module.....	27
4.3.5 Interaction Module.....	28
4.3.6 Load Module.....	28
4.3.7 Mesh Module.....	28
4.3.8 Job Module.....	29
4.3.9 Visualization Module.....	29
4.4 ABAQUS Verification.....	29
4.4.1 Boundary Condition Verification.....	32
4.5 Stress Intensity Factor Computation for SNDB.....	33
4.5.1 Geometry and Boundary Conditions.....	33
4.5.2 Stress Intensity Factor Results for SNDB Specimens .....	37
4.6 Stress Intensity Factor Change With Specimen Diameter.....	41
5. LABORATORY WORK.....	43
5.1 Mechanical Properties of Specimens.....	43
5.1.1 Pink-Gray Coloured Ankara Andesite .....	43
5.1.2 Afyon Marble.....	45
5.2 Preperation of Fracture Toughness Specimens.....	45
5.3 Compressive Loading System.....	48
5.4 Data Acquisition System.....	49
5.5 SNDB Specimens.....	51
5.5.1 Span Length Analysis for Andesite.....	53
5.5.2 Specimen Height Analysis of Andesite.....	53

5.5.3 Specimen Height Analysis of Marble.....	53
6. RESULTS & DISCUSSION.....	54
6.1 Computation Technique for SNDB Specimens.....	54
6.2 Results of Changing Span Analysis for Andesite SNDB Specimens.....	57
6.3 Results of Specimen Height Analysis of Andesite.....	61
6.4 Results of Specimen Height Analysis for Marble.....	70
6.5 SCB Tests on Andesite and Marble.....	75
6.6 Stress Distribution Around the Notch Tip.....	77
7. CONCLUSION.....	80
7.1 Recommendations.....	81
REFERENCES.....	82
APPENDICES	
A. SPECIMEN DIMENSIONS TABLES.....	86
A.1 Specimen Height Effect on Fracture Toughness Analysis for Andesite.....	86
A.2 Specimen Height Effect on Fracture Toughness Analysis for Marble.....	88
A.3 SCB Specimens for Comparing Results.....	89
B. SPECIMEN FRACTURE TOUGHNESS RESULTS TABLES.....	90
B.1 All Specimen Results of Fracture Toughness For Andesite .....	90
B.2 Average Results of Fracture Toughness For Andesite .....	91
C. SPECIMEN PHOTOS AFTER EXPERIMENTS.....	93
C.1 SNDB Ankara Andesite Specimens Photos After Experiments.....	93
C.2 SNDB Afyon Marble Specimens Photos After Experiments.....	94
C.3 SCB Specimens Photos After Experiments.....	94

## LIST OF TABLES

Table 4.1 Dimensions and mechanical properties of the single edge crack model....	31
Table 4.2 Normalized Mode I stress intensity factors for the SNDB specimens with D = 75 mm.....	37
Table 4.3 SIF change with diameter for SNDB specimens.....	41
Table 5.1 Indirect tensile strength test data and results for Brazilian Test .....	44
Table 5.2 Average Dimensions of S/R=0.6 SNDB Specimens .....	53
Table 6.1 Results of S/R=0.6 andesite specimens.....	58
Table 6.2 Results of S/R=0.7 andesite specimens.....	62
Table 6.3 Results of S/R=0.6 marble specimens.....	71
Table 6.4 Results of marble SCB specimens.....	75
Table 6.5 Results of andesite SCB specimens.....	75
Table A.1 Average dimensions of S/R=0.6 andesite SNDB specimens.....	88
Table A.2 Average dimensions of S/R=0.7 andesite SNDB specimens.....	88
Table A.3 Average dimensions of S/R=0.8 andesite SNDB specimens.....	88
Table A.4 Average dimensions of S/R=0.9 andesite SNDB specimens.....	89
Table A.5 Dimensions of S/R=0.6 marble SNDB specimens.....	90
Table A.6 Dimensions of andesite SCB Specimens.....	91
Table A.7 Dimensions of marble SCB Specimens.....	91
Table B.1 Results of S/R=0.8 andesite specimens.....	92
Table B.2 Results of S/R=0.9 andesite specimens.....	93
Table B.3 Results of S/R=0.6 andesite Specimens (Average Values).....	93
Table B.4 Results of S/R=0.7 andesite Specimens (Average Values).....	94
Table B.5 Results of S/R=0.8 andesite Specimens (Average Values).....	94
Table B.6 Results of S/R=0.9 andesite Specimens (Average Values).....	94

## LIST OF FIGURES

Figure 2.1 Fracture modes.....	8
Figure 2.2 Crack tip stress components of Mode I .....	9
Figure 2.3 Crack tip stress components of Mode II.....	10
Figure 2.4 Crack tip stress components of Mode III.....	10
Figure 2.5 Infinite plate with a center through crack under tension.....	11
Figure 2.6 Infinite plate with a hole and symmetric double through cracks under tension.....	12
Figure 2.7 Semi-infinite plate with an edge through crack under tension.....	12
Figure 2.8 Infinite stripe with a center through crack under tension.....	13
Figure 2.9 Single edge notched specimen under tension.....	13
Figure 2.10 Double edge notched specimen under tension.....	13
Figure 3.1 CCNBD under diametrical compression (Chang et al., 2001).....	16
Figure 3.2 Loading setup for fracture testing on CNBD specimen (Khan and Al-Shayea, 2000).....	17
Figure 3.3 Short Rod Specimen (Sousa & Bittencourt, 2001).....	18
Figure 3.4 Dimensions of the Chevron Bend Specimen (Ouchterlony, 1988).....	19
Figure 3.5 SNBD Specimens (Al-Shayea, 2002).....	21
Figure 3.6 Loading setup for fracture testing on SNSCB specimen (Khan and Al-Shayea, 2000).....	22
Figure 4.1 Verification problem sketch.....	29
Figure 4.2 Abaqus solution of the problem.....	30
Figure 4.3 Boundary conditions of verification.....	32
Figure 4.4 SNDB geometry.....	34
Figure 4.5 Boundary conditions.....	34
Figure 4.6 Reference point constraint.....	35
Figure 4.7 Applied load.....	35
Figure 4.8 Crack front and direction.....	36

Figure 4.9 Average normalized SIF versus normalized height of the andesite specimen, B/D.....	38
Figure 4.10 Average normalized SIF versus loading span length for andesite.....	39
Figure 4.11 Normalized SIF versus normalized height for the marble specimen....	40
Figure 4.12 Normalized SIF versus diameter of the specimen.....	42
Figure 5.1 UCS test: andesite specimen with circumferential and axial extensometer.....	44
Figure 5.2 UCS test marble specimen with circumferential and axial extensometer.	45
Figure 5.3 Smartcut 1004.....	46
Figure 5.4 Goniometer.....	46
Figure 5.5 Opening of notch in Smartcut 1004.....	47
Figure 5.6 Example SNDB code for andesite and marble respectively.....	47
Figure 5.7 Specimen and loading setup.....	48
Figure 5.8 DBK80 Analog Multiplexer, DBK43 and DBK43A strain-gage cards....	49
Figure 5.9 DaqView program window and load and displacement readings.....	50
Figure 5.10 SNDB specimen with steel rollers before the experiment.....	51
Figure 5.11 SNDB specimen geometry.....	52
Figure 6.1 Fracture toughness versus span ratio for andesite.....	59
Figure 6.2 Average fracture toughness versus span ratio for andesite.....	60
Figure 6.3 Fracture toughness versus normalized height of the andesite specimen for different S/R ratios separately.....	64
Figure 6.4 Fracture toughness versus normalized height of the andesite specimen...	65
Figure 6.5 Average fracture toughness of S/R= 0.6 and 0.7 andesite specimens .....	66
Figure 6.6 Average fracture toughness versus average specimen height/notch length for all andesite specimen groups.....	67
Figure 6.7 Fracture toughness versus height/diameter ratio for all tests on andesite.	68
Figure 6.8 Average fracture toughness versus average height/diameter ratio for andesite specimens with S/R = 0.6 and 0.7.....	69
Figure 6.9 Average fracture toughness versus average height/diameter ratio for all andesite specimens.....	70
Figure 6.10 Fracture toughness versus normalized height of the marble specimen, B/a.....	73

Figure 6.11 Fracture toughness versus normalized height of the marble specimen, B/D.....	74
Figure 6.12 Fracture toughness versus normalized height of the specimen.....	76
Figure 6.13 Horizontal stress versus distance in y-direction from the notch front ...	77
Figure 6.14 Detailed view of horizontal stress versus distance in y-direction close to the notch front.....	78
Figure 6.15 Vertical stress versus distance in y-direction from the notch front.....	79
Figure C.1 Andesite SNDB specimens after experiments according to S/R.....	95
Figure C.2 Marble SNDB specimens after experiments.....	96
Figure C.3 Andesite and marble SCB specimens after experiments.....	96

## SYMBOLS AND ABBREVIATIONS

$a$	: Crack length
$B$	: Specimen height
BDT	: Uncracked Brazilian Disk Test
CB	: Chevron Bend
CCBD	: Central Cracked Brazilian Disc under diametral compression test
CCP	: Centre Cracked Panel
CNBD	: Chevron-Notched Brazilian Disc
CNSCB	: Chevron-Notched Semi-Circular Bend
CT	: Compact Tension Test
CTOD	: Crack Tip Opening Displacement
$C_k$	: Correction factor to account for the size variation
$D$	: Specimen diameter
$E$	: Young's Modulus
EPFM	: Elastic Plastic Fracture Mechanics
$F_{max}$	: Failure load
$G$	: Strain energy release rate
ISRM	: International Society for Rock Mechanics
$J$	: J-integral
$K_{comp.}$	: Computed stress intensity factor
$K_{anal.}$	: Analytical solution for the stress intensity factor
$K_{IC}$	: Fracture toughness
$K_I$	: Stress intensity factor in Mode I
$K_{II}$	: Stress intensity factor in Mode II
$K_{III}$	: Stress intensity factor in Mode III
$L$	: Element size
LEFM	: Linear Elastic Fracture Mechanics
$P$	: Applied load
$P_{cr}$ or $P_{max}$	: Critical load

R	: Specimen radius
S	: Support span
SC3PB	: Single edge straight through cracked rectangular plate in three-point bending test
SCB	: Semi-Circular specimen under three-point Bending
SECB	: Single Edge Cracked Beam under three-point bending
SECBD	: Single edge cracked Brazilian disk in diametral compression
SECRBB	: Single Edge Cracked Round Bar Bend
SENRBB	: Single Edge Notched Round Bar in Bending
SNBD	: Straight-Notched Brazilian Disc
SNDB	: Straight-Notched Disc specimen under three-point Bending
SNSCB	: Straight-Notched Semi-Circular Bend
SR	: Short Rod
$T_0$	: Tensile strength
u	: Displacement
UCS	: Uniaxial Compressive Strength
W	: Strain energy density
$Y_I$	: Normalized stress intensity factor in Mode I
$Y_{II}$	: Normalized stress intensity factor in Mode II
$Y_{III}$	: Normalized stress intensity factor in Mode III
$Y_{min}^*$	: Critical dimensionless stress intensity factor
$\varepsilon$	: Strain
$\mu$	: Shear modulus
$\sigma$	: Stress
$\sigma_A$	: Applied stress
$\sigma_{ij}$	: Stress matrix
$\sigma_{CR}$	: Maximum tangential stress criterion
$\nu$	: Poisson's Ratio
$\Delta a_0$	: Initial position of chevron notch apex
$\Delta W$	: Variation in specimen height
$\Delta \theta$	: Chevron notch angle

# CHAPTER 1

## INTRODUCTION

### 1.1 General

Fracture mechanics is a method for predicting failure of a structure containing a crack. It uses methods of analytical solid mechanics to calculate the driving force on a crack and those of experimental solid mechanics to characterize the material's resistance to fracture. Many sciences and engineering disciplines such as Materials and Medical Sciences, Aerospace Engineering, Mechanical Engineering, Civil Engineering, Geological Engineering, Petroleum Engineering and Mining Engineering have to consider fracture mechanics in their application fields.

In modern materials science, fracture mechanics is an important tool in improving the mechanical performance of materials and components. It applies the physics of stress and strain, in particular the theories of elasticity and plasticity, to the microscopic crystallographic defects found in real materials in order to predict the macroscopic mechanical failure of bodies.

One of the fracture mechanics branches is rock fracture mechanics. Earth sciences like petroleum engineering, geological engineering and mining engineering cope with rock fracture mechanics. Finding wide application in the field of hydraulic fracturing, blasting, rock fragmentation and in many other practical problems, Mode I fracture toughness is an important property for rocks.

The explosion in rock fracture mechanics research has touched many diverse areas including blasting, hydraulic fracturing and in situ stress determination, mechanical fragmentation, rock slope analysis, earthquake mechanics, earthquake prediction, plate tectonics, magmatic intrusions, hot dry rock geothermal energy extraction, fluid

transport properties of fracturing rock masses, propagating oceanic rifts, crevasse penetration and other glaciological problems, the development of steeply dipping extension fractures that are nearly ubiquitous at the earth's surface and are formed through folding, upwarping and rifting and the modeling of time-dependent rock failure, (Atkinson, 1987; Whittaker et al., 1992).

## **1.2 Statement of the Problem and the Thesis Objective**

In this study a new testing technique for fracture testing of rock cores is used to investigate the applicability of this specimen geometry to other rock types. To determine fracture toughness, experiments were performed on discs. Three-point bending was used as the loading method. Disc with three-point bending that is Straight Notched Disc Specimen Under Three-Point Bending (SNDB) method, which is a new method, was employed to determine the Mode I fracture toughness of the pink colored Ankara Andesite from Gölbaşı and Afyon Marble. With this new method, investigation of effects of specimen height and changing span on fracture toughness and stress intensity factor is carried out. Afyon Marble specimens were added to the testing program to check the applicability of this new fracture testing technique for other rock types.

## **1.3 Methodology**

Middle East Technical University licentate software ABAQUS (Three dimensional finite element program) was used to determine the stress intensity factors of the specimens. Every specimen was introduced to the software models by its own dimensions. This way, variations in the stress intensity factors due to differences in the specimen dimensions that occurred during specimen preparations were taken into account.

Cylindrical core specimens had an approximately 75 mm diameter and 37.5 mm radius. The height of the specimens was varied from 17 mm - 67 mm in order to find the ideal specimen height range for Mode I testing with SNDB specimens. Initial notch introduced to initiate crack propagation in the discs had a length of around 10 mm.

Effect of specimen height was studied by changing height of the specimens from 17 mm to 67 mm. Specimen heights tried were 17, 27, 37, 47, 57 and 67 mm for andesite and 27, 32, 37, 47, 52 and 54 mm for marble. A total of 64 tests were carried out for andesite samples, 4 tests for each thickness. A total of 19 tests were conducted for marble.

For andesite specimens loading span was changed and effect of variation of span between  $S/R = 0.6$  to  $0.9$  was studied for 4 different  $S/R$  values with about 16 tests at each  $S/R$  ratio.

Fracture toughness values were evaluated by using the stress intensity factors computed from numerical modeling and crack initiation loads of the experiments.

### ***1.4 Sign Convention***

In this study, on the contrary to the general rock mechanics convention, compressive stresses are taken negative and the tensile stresses are taken positive. The reason for this ABAQUS finite element program used extensively in this work is a general engineering program with a regular solid mechanics sign convention. Coordinate axes marked with 1, 2 and 3 in ABAQUS according to the general tensor notation correspond to x, y and z axes, respectively.

## **1.5 Outline of the Thesis**

In Chapter 2, historical overview of the fracture mechanics is presented. Fracture criteria, fracture parameters and loading modes are introduced in Chapter 2. In Chapter 3 fracture test techniques that are used extensively are reviewed. 3D Numerical modeling of the specimens and calculations of stress intensity factor are presented in Chapter 4. Laboratory work with experimental setup is given in Chapter 5. Results and graphs are presented in Chapter 6. Conclusion is in Chapter 7.

## CHAPTER 2

# FRACTURE MECHANICS

### 2.1 Historical Overview

The commonly accepted first successful analysis of a fracture-dominant problem was that of Griffith in 1920, who considered the propagation of brittle cracks in glass. Griffith formulated the well-known concept that an existing crack will propagate if thereby the total energy of the system is lowered, and he assumed that there is a simple energy balance, consisting of a decrease in elastic strain energy within the stressed body as the crack extends, counteracted by the energy needed to create the new crack surfaces. His theory allows the estimation of the theoretical strength of the brittle solids and also gives the correct relationship between the fracture strength and defect size, (Janssen et al., 2002).

The Griffith concept was first related to brittle fracture of metallic materials by Zener and Hollomon in 1944. Soon after, Irwin pointed out that the Griffith-type energy balance must be between the stored strain energy and the surface energy plus the work done in plastic deformation. Irwin defined the “energy release rate” or “crack driving force”,  $G$ , as the total energy that is released during cracking per unit increase in crack size. He also recognised that for relatively ductile materials the energy required to form new crack surfaces is generally insignificant compared to the work done in plastic deformation, (Janssen et al., 2002).

In the middle 1950s Irwin contributed another major advance by showing that the energy approach is equivalent to the stress intensity ( $K$ ) approach, according to which fracture occurs when a critical stress distribution ahead of the crack tip is reached. The material property governing fracture may therefore be stated as a

critical stress intensity,  $K_c$ , or in terms of energy as a critical value  $G_c$ , (Janssen et al., 2002).

After the fundamentals of fracture mechanics were established around 1960, scientists turned their attention on the plasticity of the crack tips. During this time period several researchers developed analyses to correct for yielding at the crack tip, including Irwin (1961), Dugdale (1960), Barenblatt (1962) and Wells (1961). The Irwin (1961) plastic zone correction was relatively simple extension of LEFM, while Dugdale (1960) and Barenblatt (1962) each developed somewhat more elaborate models based on a narrow strip of yielded material at the crack tip. On the other hand Wells (1961) proposed the displacement of the crack faces as an alternative fracture criterion when significant plasticity precedes failure. He attempted to apply LEFM to low- and medium-strength structural steels. These materials were too ductile for LEFM to apply, but Wells noticed that the crack faces moved apart with plastic deformation. This observation led to the development of the parameter now known as the crack tip opening displacement (CTOD), (Anderson, 1991).

In 1968, Rice (1968) modeled the plastic deformation as nonlinear elastic behavior and extended the method of energy release rate to nonlinear materials. He showed that the energy release rate can be expressed as a path-independent line integral, called the  $J$  integral. Rice's theory has since dominated the development of fracture mechanics in United States. During his study was being published, Rice discovered that Eshelby (1956) had previously published several so-called conservation integrals, one of which was equivalent to Rice's  $J$  integral. However, Eshelby (1956) did not apply his integrals to crack problems. In 1971 Begley and Landes (1972) who were research engineers at Westinghouse, came across Rice's article and decided to characterize fracture toughness of these steels with the  $J$  integral. Their experiments were very successful and led to the publication of a standard procedure for  $J$  testing of metals ten years later. In 1976, Shih and Hutchinson (1976) established a fracture design analysis based on the  $J$  integral by providing the theoretical framework for such an approach. In addition to this analysis Shih demonstrated a relationship

between the J integral and the CTOD, implying that both parameters are equally valid for characterizing fracture, (Anderson, 1991).

Fracture mechanics basically can be divided into two main categories. These are:

- 1) Linear Elastic Fracture Mechanics (LEFM),
- 2) Elastic-Plastic Fracture Mechanics (EPFM).

## **2.2 Linear Elastic Fracture Mechanics**

Demonstration of the equivalence of G and K provided the basis development of the discipline of Linear Elastic Mechanics. This is because the form of the stress distribution around and close to a crack tip is always the same. (Janssen et al., 2002)

Linear elastic fracture mechanics has been developed to describe crack growth and fracture within a material under essentially linear elastic conditions. It is based on the assumption that the influence of applied loads upon crack extension can be represented in terms of certain parameters that characterize the stress-strain intensity near the crack tip, (Soo-Ho Chang et al., 2001).

Linear Elastic Fracture Mechanics (LEFM) first assumes that the material is isotropic and linear elastic. Based on the assumption, the stress field near the crack tip is calculated using the theory of elasticity. When the stresses near the crack tip exceed the material fracture toughness, the crack will grow.

## 2.3 Loading Modes

Fracture classification is based on the fracture mode terminology of classical fracture mechanics. Three basic failure modes are possible in fracture mechanics. These are Mode I, Mode II and Mode III, (Figure 2.1), (Irwin,1958).

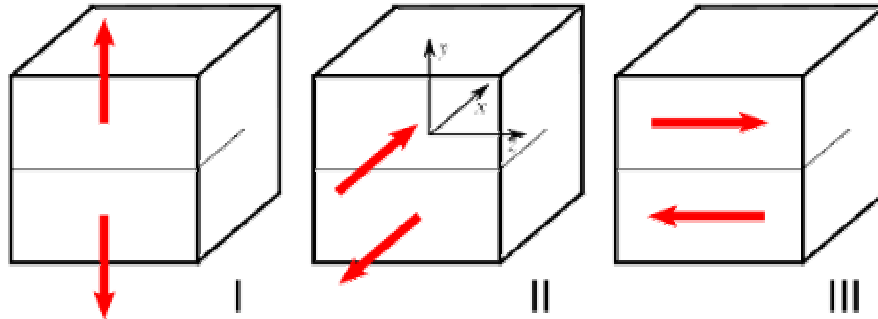


**Figure 2.1** Fracture modes

**Mode I crack** : Opening mode (a tensile stress normal to the plane of the crack)

**Mode II crack** : Sliding mode (a shear stress acting parallel to the plane of the crack and perpendicular to the crack front)

**Mode III crack** : Tearing mode (a shear stress acting parallel to the plane of the crack and parallel to the crack front)

## 2.4 Crack Tip Stress and Stress Intensity Factor

Stress and displacement fields near a crack tip of a linear elastic isotropic material are listed separately for all three modes: Mode I, Mode II, Mode III, in Figures 2.2, 2.3 and 2.4.

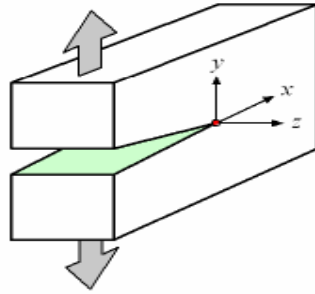
Please note that we use the Greek letter  $\mu$  to denote the shear modulus, usually written as  $G$ . Also, the small differences in formulas for plane stress and plane strain conditions are handled by  $\kappa$ , where

$$\mathbf{K} = \begin{cases} \frac{3-\nu}{1+\nu} & (\text{Plane Stress}) \\ 3-4\nu & (\text{Plane Strain}) \end{cases} \quad (2.13)$$

$r$  and  $\theta$  are the polar coordinates for an origin of x-y reference system positioned at the crack tip.

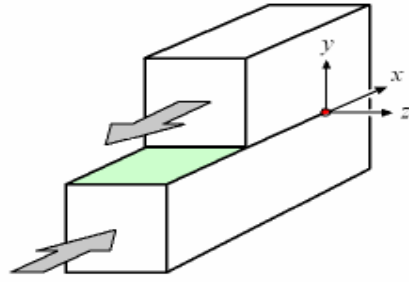
For linear elastic materials, the principle of superposition applies. A mixed-mode problem can be treated as a the summation of each mode. Using symbol  $\sigma_{ij}$  for general stres matrix:

$$\sigma_{ij}^{(Total)} = \sigma_{ij}^{(I)} + \sigma_{ij}^{(II)} + \sigma_{ij}^{(III)} \quad (2.14)$$



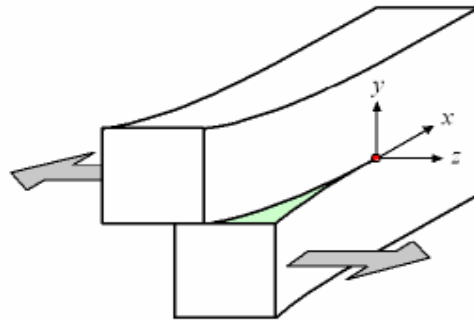
$$\begin{aligned} \sigma_{xx} &= \frac{K_I}{\sqrt{2\pi r}} \cos\left(\frac{\theta}{2}\right) \left[1 - \sin\left(\frac{\theta}{2}\right) \sin\left(\frac{3\theta}{2}\right)\right] \\ \sigma_{yy} &= \frac{K_I}{\sqrt{2\pi r}} \cos\left(\frac{\theta}{2}\right) \left[1 + \sin\left(\frac{\theta}{2}\right) \sin\left(\frac{3\theta}{2}\right)\right] \\ \sigma_{zz} &= \begin{cases} 0 & (\text{Plane Stress}) \\ \nu(\sigma_{xx} + \sigma_{yy}) & (\text{Plane Strain}) \end{cases} \\ \tau_{xy} &= \frac{K_I}{\sqrt{2\pi r}} \cos\left(\frac{\theta}{2}\right) \sin\left(\frac{\theta}{2}\right) \cos\left(\frac{3\theta}{2}\right) \\ \tau_{yz} &= 0 \\ \tau_{zx} &= 0 \\ u_x &= \frac{K_I}{2\mu} \sqrt{\frac{r}{2\pi}} \cos\left(\frac{\theta}{2}\right) \left[\kappa - 1 + 2 \sin^2\left(\frac{\theta}{2}\right)\right] \\ u_y &= \frac{K_I}{2\mu} \sqrt{\frac{r}{2\pi}} \sin\left(\frac{\theta}{2}\right) \left[\kappa + 1 - 2 \cos^2\left(\frac{\theta}{2}\right)\right] \\ u_z &= 0 \end{aligned}$$

**Figure 2.2** Crack tip stress components of Mode I



$$\begin{aligned} \sigma_{xx} &= -\frac{K_{II}}{\sqrt{2\pi r}} \sin\left(\frac{\theta}{2}\right) \left[ 2 + \cos\left(\frac{\theta}{2}\right) \cos\left(\frac{3\theta}{2}\right) \right] \\ \sigma_{yy} &= \frac{K_{II}}{\sqrt{2\pi r}} \sin\left(\frac{\theta}{2}\right) \cos\left(\frac{\theta}{2}\right) \cos\left(\frac{3\theta}{2}\right) \\ \sigma_{zz} &= \begin{cases} 0 & \text{(Plane Stress)} \\ \nu(\sigma_{xx} + \sigma_{yy}) & \text{(Plane Strain)} \end{cases} \\ \sigma_{xy} &= \frac{K_{II}}{\sqrt{2\pi r}} \cos\left(\frac{\theta}{2}\right) \left[ 1 - \sin\left(\frac{\theta}{2}\right) \sin\left(\frac{3\theta}{2}\right) \right] \\ \tau_{yz} &= 0 \\ \tau_{zx} &= 0 \\ u_x &= \frac{K_{II}}{2\mu} \sqrt{\frac{r}{2\pi}} \sin\left(\frac{\theta}{2}\right) \left[ \kappa + 1 + 2\cos^2\left(\frac{\theta}{2}\right) \right] \\ u_y &= -\frac{K_{II}}{2\mu} \sqrt{\frac{r}{2\pi}} \cos\left(\frac{\theta}{2}\right) \left[ \kappa - 1 - 2\sin^2\left(\frac{\theta}{2}\right) \right] \\ u_z &= 0 \end{aligned}$$

**Figure 2.3** Crack tip stress components of Mode II



$$\begin{aligned} \sigma_{xx} &= 0 \\ \sigma_{yy} &= 0 \\ \sigma_{zz} &= 0 \\ \tau_{xy} &= 0 \\ \tau_{yz} &= \frac{K_{III}}{\sqrt{2\pi r}} \cos\left(\frac{\theta}{2}\right) \\ \tau_{zx} &= -\frac{K_{III}}{\sqrt{2\pi r}} \sin\left(\frac{\theta}{2}\right) \\ u_x &= 0 \\ u_y &= 0 \\ u_z &= \frac{K_{III}}{\mu} \sqrt{\frac{r}{2\pi}} \sin\left(\frac{\theta}{2}\right) \end{aligned}$$

**Figure 2.4** Crack tip stress components of Mode III

$K_I$ ,  $K_{II}$ ,  $K_{III}$  are the factors depending on the outer boundary conditions, i.e. applied loading and geometry and also called as the stress intensity factor. In fracture mechanics the stress intensity factor gives the grade of stress concentration at the tip of a crack of length for a given loading and has the dimension of  $stress \times \sqrt{length}$ , in units  $MPa\sqrt{m}$ , (Backers, 2004).

$$K_{I, II, III} = \sigma_A \sqrt{\pi \times a} = \sigma_{ij} \sqrt{2\pi \times r}; \text{ for } \theta = 0 \quad (2.16)$$

where,

$\sigma_A$ : Applied Stress

a: Crack Length

Some typical stress intensity factor  $K_I$  solutions for the best known loading conditions are shown in Figures 2.5 - 2.10.

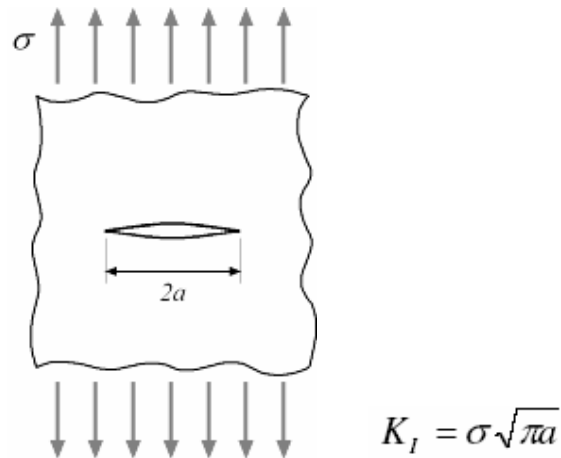


**Figure 2.5** Infinite plate with a center through crack under tension

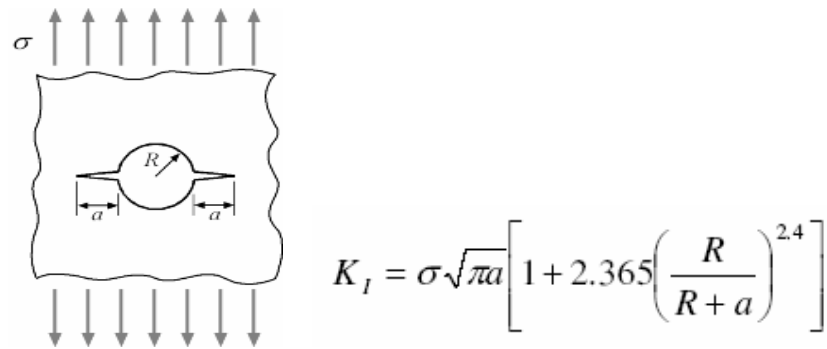


**Figure 2.6** Infinite plate with a hole and symmetric double through cracks under tension

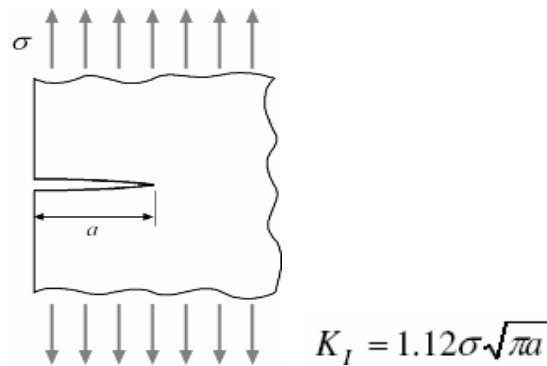


**Figure 2.7** Semi-infinite plate with an edge through crack under tension

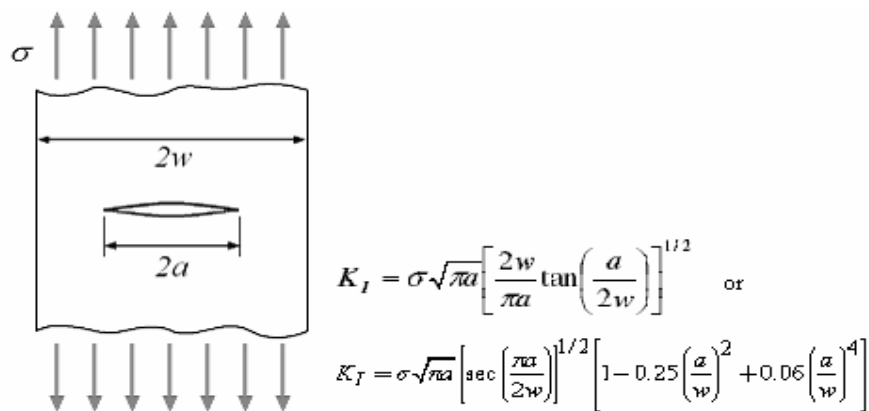
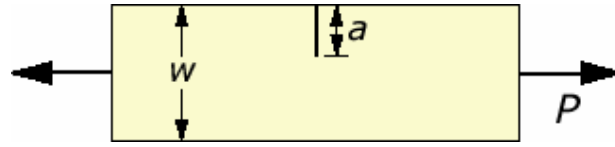
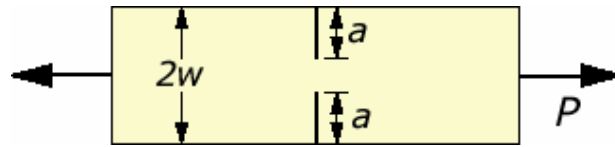


**Figure 2.8** Infinite stripe with a center through crack under tension



$$K_I = \frac{P}{B\sqrt{w}} \left[ \frac{\sqrt{2 \tan\left(\frac{\pi a}{2w}\right)}}{\cos\left(\frac{\pi a}{2w}\right)} \left[ 0.752 + 2.02 \left(\frac{a}{w}\right) + 0.37 \left(1 - \sin\left(\frac{\pi a}{2w}\right)\right)^3 \right] \right]$$

**Figure 2.9** Single edge notched specimen under tension



$$K_I = \frac{P}{B\sqrt{w}} \left[ \frac{\sqrt{\frac{\pi a}{2w}}}{\sqrt{1 - \frac{a}{w}}} \left[ 1.122 - 0.561 \frac{a}{w} - 0.205 \left(\frac{a}{w}\right)^2 + 0.471 \left(\frac{a}{w}\right)^3 + 0.190 \left(\frac{a}{w}\right)^4 \right] \right]$$

**Figure 2.10** Double edge notched specimen under tension

## 2.5 Fracture Criteria

Griffith was the first to derive a formula relating the critical values of crack length,  $a_c$ , and applied stress,  $\sigma_c$ , on the basis of an energy balance concept, (Rossmannith, 1983).

The Griffith criterion states that crack growth will occur when the strain energy release by a virtual extension of the crack exceeds the energy absorbed by the material in that crack advance. The energy absorbed in crack propagation is assumed

to be constant for a given material and includes plasticity and free surface energy, (Rossmanith, 1983).

## **2.6 Fracture Toughness**

An engineering approach is to perform a series of experiments and reach at a critical stress intensity factor  $K_C$  for each material, this critical parameter is known as the fracture toughness. When measured under certain conditions this parameter has been shown to be a true material constant for a great many materials, (Rossmanith, 1983).

$K_{IC}$  can be considered a material property characterizing the crack resistance, and is therefore called the plane strain fracture toughness. Thus the same values of  $K_{IC}$  should be found by testing specimens of the same material with different geometries and with critical combinations of crack size and shape and fracture stress. Within certain limits this is indeed the case, and so a knowledge of  $K_{IC}$  obtained under standard conditions can be used to predict failure for different combinations of stress and crack size and for different geometries, (Janssen et al., 2002).

$K_C$  can be determined under standard conditions, and the values thus found may also be used to predict failure, but only for situations with the same material thickness and constraint, (Janssen et al., 2002).

## **2.7 Elastic Plastic Fracture Mechanics**

Linear Elastic Fracture Mechanics can deal with only limited crack tip plasticity, *i.e.* the plastic zone must remain small compared to the crack size and the cracked body as a whole must still behave in an approximately elastic manner. If this is not the case then the problem has to be treated elasto-plastically. Due to its complexity the concepts of Elastic-Plastic Fracture Mechanics (EPFM) are not so well developed as LEFM theory, a fact is reflected in the approximate nature of the eventual solutions, (Janssen et al., 2002).

## **CHAPTER 3**

### **ROCK FRACTURE TESTING ON DISC TYPE SPECIMENS**

In order to assess the stress intensity factor under Mode I conditions, International Society for Rock Mechanics (ISRM) suggests three methods which use following specimen types:

- Chevron-Notched Brazilian Disc (CCNBD) Specimens
- Short Rod (SR) Specimens
- Chevron Bend (CB) Specimens

Some of the additional testing methods used in the previous work to find fracture toughness use the following specimen types for which stress intensity evaluations are given in the related literature:

- Straight-Notched Brazilian Disc (SNBD) Specimens
- Straight-Notched Semi-Circular Bend (SNSCB) Specimens
- Punch Through Shear (PTS) Tests

#### **3.1 Cracked Chevron-notched Brazilian Disc (CCNBD) Specimens**

The Cracked Chevron-Notched Brazilian Disc (CCNBD) Specimen (Figure 3.1), has the same geometry and shape as the conventional Brazilian disc used for measuring the indirect tensile strength of rock, except that the CCNBD specimen has a chevron notch. Shetty et al. (1985) first used it for measuring the fracture toughness of ceramics, and applied the stress intensity factor solutions of a cracked straight-through Brazilian disc (CSTBD) with a through notch to the CCNBD by means of

the straight-through crack assumption (STCA) method. Afterwards, ISRM presented the suggested method for determining Mode I fracture toughness using a CCNBD specimen because it has many advantages over other methods, (Fowell, 1995). But this yields a solution only for mode I fracture toughness, (Chang et al., 2001).

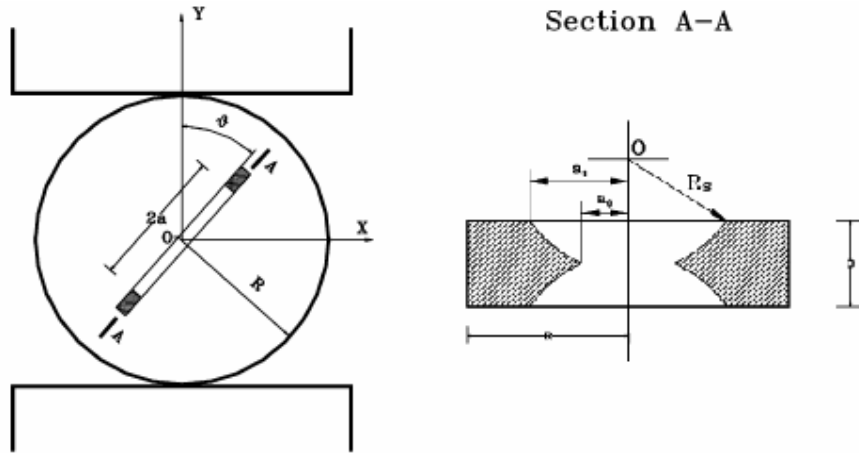


**Figure 3.1** CCNBD under diametrical compression (Chang et all, 2001)

The chevron notch is made with two cuts from both sides of the disc along the disc rotating axis on the same diametrical cutting plane, which is to be the designed crack orientation direction. First, the gap is set between the disc surface and the rotating wheel to zero. The first cut is made by moving the disc toward the rotating wheel up to the designed cutting depth. After this cut, the specimen together with the fixture are removed from the fixing vice and turned  $180^{\circ}$ . The specimen is cut to the same depth as the first cut, (Figure 3.1). The cutting depth is determined according to the specimen radius and the designed dimensionless geometric parameters such as  $a_0$ ,  $a_1$  or  $a_B$ , (Chang et all, 2001).

Fracture toughness is calculated by using expression suggested by ISRM (1995). The expression is in Equation 3.1.

$$K_{IC} = \frac{P_{\max}}{B\sqrt{D}} Y_{\min}^* \quad (3.1)$$

where  $D$  is the diameter,  $B$  is the thickness of the specimen,  $P_{\max}$  is the compressive load at failure,  $Y_{\min}^*$  is the critical dimensionless stress intensity factor.

A strain-controlled loading frame is used for the load application. The applied load and load point displacement are obtained using a computerized data logger, (Figure 3.2).

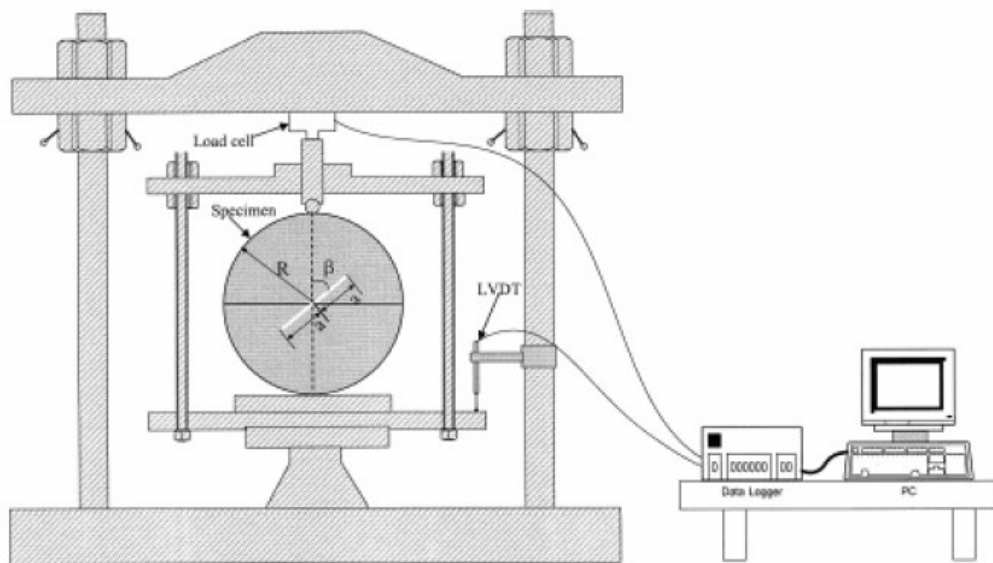


**Figure 3.2** Loading setup for fracture testing on CNBD specimen (Khan and Al-Shayea, 2000)

### 3.2 Short Rod (SR) Specimens

Short Rod specimen was developed by Barker (1977). In SR specimen, a chevron notch is cut in cylindrical specimen and fracture toughness computation is done by an analytical method which is achieved by ISRM (1988) and a correction factor for the nonlinear behavior of the material is calculated with another equation depending on the Load-CMOD curve of the fracture experiments. SR method is only used to determine Mode I fracture toughness, (Sousa & Bittencourt, 2001).

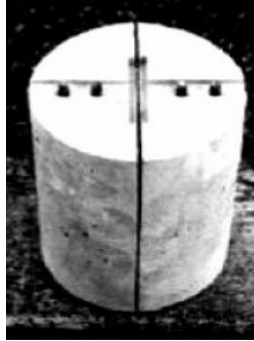


**Figure 3.3** Short Rod Specimen (Sousa & Bittencourt, 2001)

The cylindrical samples are obtained from cored blocks. In order to provide loading surface in tension, a rectangular grip groove is machined in one end of the short rod specimen. After grip groove is opened, two slots are cut at opposing angles. Moreover, these slots must form a triangular ligament which is called as chevron.

For Level 1 testing, according to the ISRM (1988), fracture toughness of the SR specimen is accomplished by Equation 3.2.

$$K_{SR} = C_K 24.0 F_{\max} / D^{1.5} \quad (3.2)$$

where  $F_{\max}$  is the failure load,  $D$  is the specimen diameter and  $C_K$  is the correction factor to account for the size variation of the specimen;

$$C_K = \left( 1 - \frac{0.6\Delta W}{D} + \frac{1.4\Delta a_0}{D} - 0.01\Delta\theta \right) \quad (3.3)$$

where,

$\Delta W$  = variation in specimen height

$\Delta a_0$  = initial position of chevron notch apex

$\Delta\theta$  = chevron notch angle

Afterward a nonlinearity correction factor is calculated and corrected fracture toughness of SR specimen is evaluated.

### 3.3 Chevron Bend (CB) Specimens

3 point bending loading for determination of Mode I fracture toughness,  $K_{IC}$ , is applied according to the ISRM Suggested Method, (Ouchterlony, 1988), using the Chevron Bend (CB) method. The dimensions are outlined in Figure 3.4

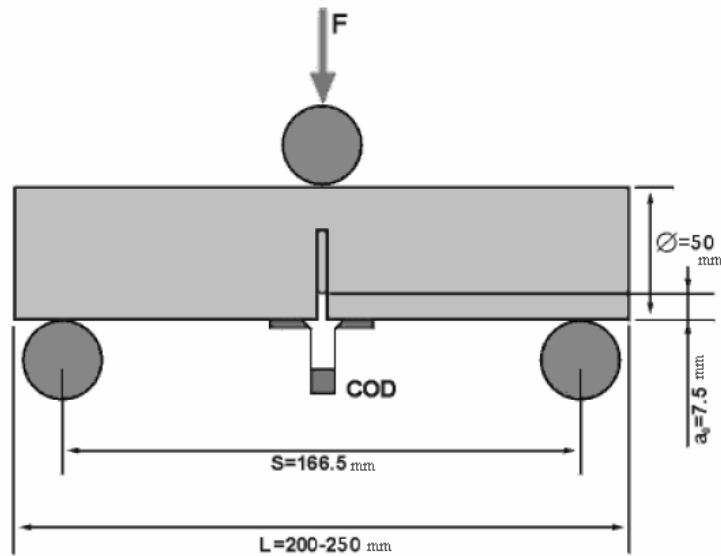


**Figure 3.4** Dimensions of the Chevron Bend Specimen (Ouchterlony, 1988)

Core samples of desired diameter are used in this study. A chevron (V-) shaped notch is cut in the middle of the specimen meeting the requirements. Centred to the notch tip two metal knives are glued on the mantle surface using a quick hardening glue. A clip-gage for measuring the notch opening (clip-gage opening displacement, COD) is attached to the knives. For accurate measurement of sample bending (load-point displacement,  $l_{pd}$ ) a saddle equipped with  $l_{vdt}$ 's (linear variable differential transformers) can be applied, resting on top of the sample. AE transducers are

directly glued to the sample surface. The assembly is placed centred with respect to the notch onto two support rollers. The tip of the notch is pointing downwards. A third roller applies the load opposite the notch tip inducing a three-point bending to the core specimen, (Modified from Backers, 2004). Equations 3.2 and 3.3 are used to calculate fracture toughness of CB.

### **3.4 Straight-Notched Brazilian Disc (SNBD) Specimens**

Chong and Kuruppu (1984) developed the Straight-Notched Brazilian Disc Specimen (SNDB) method. In SNBD specimen, straight notch is opened to circular disc with drill bit and wire saw. By using a mathematical expression fracture toughness is calculated. Stress intensity factor is included in this expression, which is determined by using numerical methods.

Mode I, Mode II and mixed mode fracture toughness determination are possible by using SNBD method.

Firstly, cores are obtained from the rock blocks. They are cut into circular discs, using a high speed diamond plated rotary saw. The sliced discs are sanded to ensure uniform thickness. Then a hole is initially drilled at the center of the discs using a drilling bit in a lathe. The bit is made to penetrate the rotating disc to the midthickness of the specimen, afterward the disk is reversed and the hole is completed. The wire of the saw is passed through the drilled hole and a notch of any length is machined in the disk. The depth of the cut is precisely controlled by a moving platform on which specimen is mounted, (Figure 3.5). Testing equipment and setup are similar to that of CNBD specimen test, (Figure 3.2).

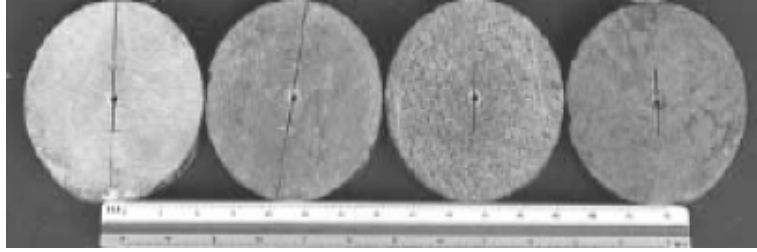


**Figure 3.5** SNBD specimens (Al-Shayea, 2002)

For fracture toughness computation, stress intensity factor in Equation 3.4 is used, (Atkinson et al., 1982).

$$K_I = \frac{P\sqrt{a}}{\sqrt{\pi RB}} N_I \quad (3.4)$$

where,

$K_I$  = stress intensity factor in Mode I

$R$  = radius of the Brazilian disc

$B$  = thickness of the specimen

$P$  = compressive load at failure

$N_I$  = non-dimensional coefficients which depend on  $a/R$

For  $N_I$ , Equation 3.5 was derived by Shetty and Rosenfield (1985) by fitting the numerical results of Atkinson et al. (1982).

$$N_I = 0.99 + 0.141\left(\frac{a}{R}\right) + 0.863\left(\frac{a}{R}\right)^2 + 0.886\left(\frac{a}{R}\right)^3 \quad (3.5)$$

### 3.5 Straight-Notched Semi Circular Bending (SNSCB) Specimens

Straight-Notched Semi Circular Bending Specimen (SNSCB) technique was advocated by Lim et al. (1994). SNSCB specimen is obtained from a half disc. A straight notch is cut into half disc. Fracture toughness is determined from an equation which depends on a numerical constant, normalized stress intensity factor. SNSCB specimen can be used for Mode I, Mode II and mixed mode studies.

SNSCB type specimen testing geometry developed by Chong and Kuruppu (1984), has a single edge notch of length  $a$  and is loaded in a three-point bending configuration (Figure 3.6). SCB is especially suitable for applications requiring duplicate samples having similar composition, as such circular discs provide two duplicate specimens. Furthermore, the SCB can be used to study mixed-mode fracturing, by cutting a crack at an angle, (Chong and Kuruppu, 1989).

An example loading setup is shown in Figure 3.7 which was used by Khan and Al-Shayea for SNSCB testing

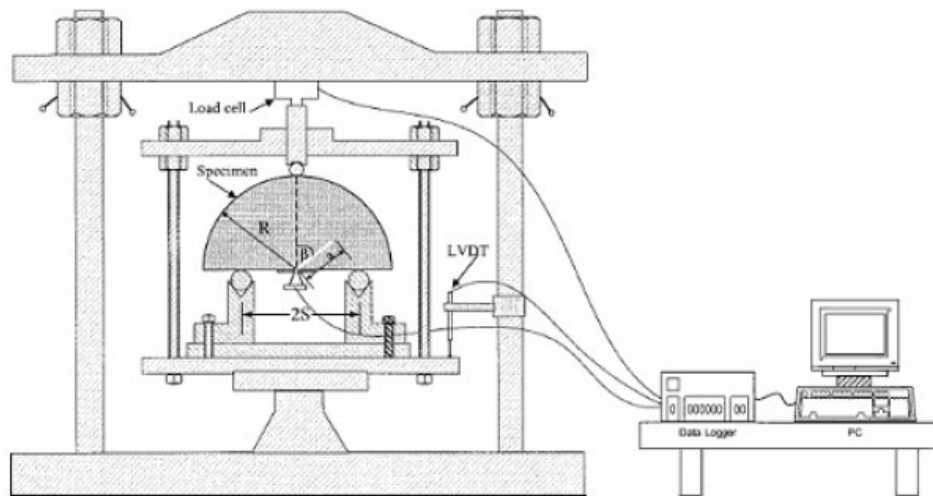


**Figure 3.6** Loading setup for fracture testing on SNSCB specimen (Khan and Al-Shayea, 2000)

To estimate fracture toughness in Mode I, firstly, normalized stress intensity factor is calculated with Equation 3.6. The stress intensity factor in the equation is achieved by using numerical methods.

$$Y_I = \frac{K_I}{\sigma_0 \sqrt{\pi a}} \quad (3.6)$$

where  $Y_I$  is the normalized stress intensity factor,  $K_I$  is the stress intensity factor  $a$  is the notch or crack length. Stress  $\sigma_0$  corresponds to the stress distributed to the bottom boundary of the sample and is given by:

$$\sigma_0 = \frac{P}{2RB} \quad (3.7)$$

where  $P$  is the failure load,  $R$  is the specimen radius and  $B$  is the specimen thickness.

By using the normalized stress intensity factor, fracture toughness of the rock is calculated with the Equation 3.8.

$$K_{IC} = Y_I \sigma_{cr} \sqrt{\pi a} \quad (3.8)$$

where:

$Y_I$ : Normalized stress intensity factor

$a$ : Notch length

$$\sigma_{cr}: \frac{P_{cr}}{2RB}$$

$P_{cr}$ : Critical load when the fracture occurs

$R$ : Specimen radius

$B$ : Specimen thickness

### **3.6 Summary of Results of Fracture Testing on Rock Cores**

In Backers studies, the CCNBD specimen had the smallest standard deviation in Mode I fracture toughness, and the effects of the diameter, notch length and thickness on fracture toughness were negligible for the geometry and shape of the CCNBD specimen. Mode I fracture toughness values from CB and CCNBD tests showed very close relationships with one another.

Khan and Al-Shayea (2000) used SCB specimens under three-point-bending. He showed that specimen diameter and crack type had a substantial influence on the measured fracture toughness. Mode I fracture toughness is significantly influenced by specimen diameter and crack type. The Brazilian disc with a straight notch was found to be the most convenient geometry to use for fracture toughness determination.

Krishnan et al. (1997) pointed out the effect of anisotropy and bedding planes on fracture toughness. Fracture toughness can be evaluated easily by orienting the notch with respect to the area of interest in SNBD specimen.

## CHAPTER 4

# NUMERICAL MODELING FOR ESTIMATION OF STRESS INTENSITY FACTORS

For calculating stress intensity factors of the samples with different geometries, numerical computations were carried out. These computations were done by 3D Finite element program ABAQUS. ABAQUS program is chosen for its user friendly package and ease in learning and running applications with the program.

### 4.1 Finite Element Program ABAQUS

ABAQUS is a finite element (FE) program used for stress, heat transfer, and other types of analysis in structural, mechanical, civil, biomedical, and related engineering applications. ABAQUS Version 6.5 was leased by METU is used in modeling work here. Two dimensional and three dimensional fracture analyses can be performed with ABAQUS. ABAQUS uses J-Integral method to compute stress intensity factors.

With ABAQUS /CAE you can quickly and efficiently create, edit, monitor, diagnose, and visualize advanced ABAQUS analyses. The intuitive interface integrates modeling, analysis, job management, and results visualization in a consistent, easy-to-use environment that is simple to learn for new users yet highly productive for experienced users. ABAQUS /CAE supports familiar interactive computer aided engineering concepts such as feature-based, parametric modeling, interactive and scripted operation, and GUI customization, (<http://www.simulia.com/>).

ABAQUS program was written and maintained by SIMULIA. SIMULIA is the Dassault Systèmes brand that delivers a scalable portfolio of Realistic Simulation solutions including the ABAQUS product suite for Unified Finite Element

Analysis, multiphysics solutions for insight into challenging engineering problems, and lifecycle management solutions for managing simulation data, processes, and intellectual property, (<http://www.simulia.com/>).

In Turkey ABAQUS office is in Istanbul and the company name is 'A to Z Advanced Engineering Technologies' (A-Ztech Ltd.).

## **4.2 Abaqus Capabilities**

ABAQUS is a highly sophisticated, general purpose finite element program which includes:

- The ability to model very large shape changes in solids, in both two and three dimensions,
- Parts and assemblies can be created in Abaqus/CAE using the constrain-driven sketchers.
- An advanced material library, including the usual elastic and elastic – plastic solids; models for foams, concrete, soils, piezoelectric materials, and many others.
- Capabilities for both static and dynamic problems,
- It offers a comprehensive meshing environment and provides a variety of sophisticated approaches for simplifying and speeding up mesh creation.
- A very extensive element library, including a full set of continuum elements, beam elements, shell and plate elements, among others.
- A sophisticated capability to model contact between solids

### **4.3 ABAQUS Modules**

ABAQUS is a very user friendly program. In order to define the geometry and other physical properties of the model and then to submit the model for analysis, several different modules are used step by step in the program as following.

#### **4.3.1 Part Module**

Part module is used to create, edit, and manage the parts in the current model. Part module has ability to create deformable, discrete rigid or analytical rigid parts. Solids, shells, wires, cuts, and rounds can be drawn by part module.

#### **4.3.2 Property Module**

Property module is briefly used to define material properties of the model and assign this property to model.

#### **4.3.3 Assembly Module**

Assembly module is basically used to create part instances and position them relative to each other in a global coordinate system.

#### **4.3.4 Step Module**

Step module is used to perform a sequence of one or more analysis steps. The sequence of steps provides a convenient way to capture changes in the loading and boundary conditions of the model. Step module also has an ability to specify output requests. For instance, in fracture mechanics applications, to obtain stress intensity factor data at the end of the analysis, a history output request is defined in step module. Under the menu options of step module J-Integral and stress intensity factor computation options are available. Maximum tangential stress criterion, maximum

strain energy release rate criterion or  $K_{II} = 0$  criterion can be selected to calculate the crack propagation direction at initiation. Calculation of contour integrals for the evaluation of the J-integral and the stress intensity factors is carried out in a region surrounded by a number of contours specified by the user. Stress intensity factors are computed for the elements in the chosen contour region around the notch tip. Then user can request an averaging of the stress intensity factors in the chosen region to end up one single accurate value for the particular notch tip.

#### **4.3.5 Interaction Module**

Interaction module is used to satisfy mechanical and thermal interactions between regions of a model, connections between two points of a model or between a point of a model and ground. Moreover, springs and dashpots between two points of a model or between a point of a model and ground are applied by interaction module. Furthermore, to define a crack in a region interaction module is used. Crack can be defined in two ways one is sharp crack that is also called seam and the other is blunted crack.

#### **4.3.6 Load Module**

Loads and boundary conditions are defined by considering step module in Load module.

#### **4.3.7 Mesh Module**

The Mesh module is used to generate meshes on parts and assemblies of the model. Mesh attributes such as seeds, mesh techniques, and element types are determined in mesh module. In fracture tests, crack tips cause stress concentrations and stress and strain gradients are large as a crack tip is approached. Therefore, to get accurate stresses and strains, the finite element mesh must be refined in the vicinity of the crack tip.

### 4.3.8 Job Module

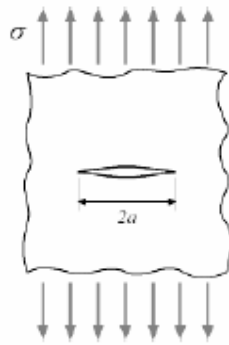
Job module is used to submit the analysis for processing. During process, job module can monitor progress of the process. Job module starts the Visualization module.

### 4.3.9 Visualization Module

Visualization module finally shows the results of the analysis in terms of deformed shapes, contours, symbols, animations, and graphs.

## 4.4 ABAQUS Verification

In order to verify and assess the accuracy and applicability of ABAQUS program for fracture mechanics computations an example problem with a known analytical solution is solved, (Figure 4.1).



$$K_I = \sigma \sqrt{\pi a}$$

(a) Infinite Plate with a Center Through Crack under Tension

**Figure 4.1** Verification problem sketch

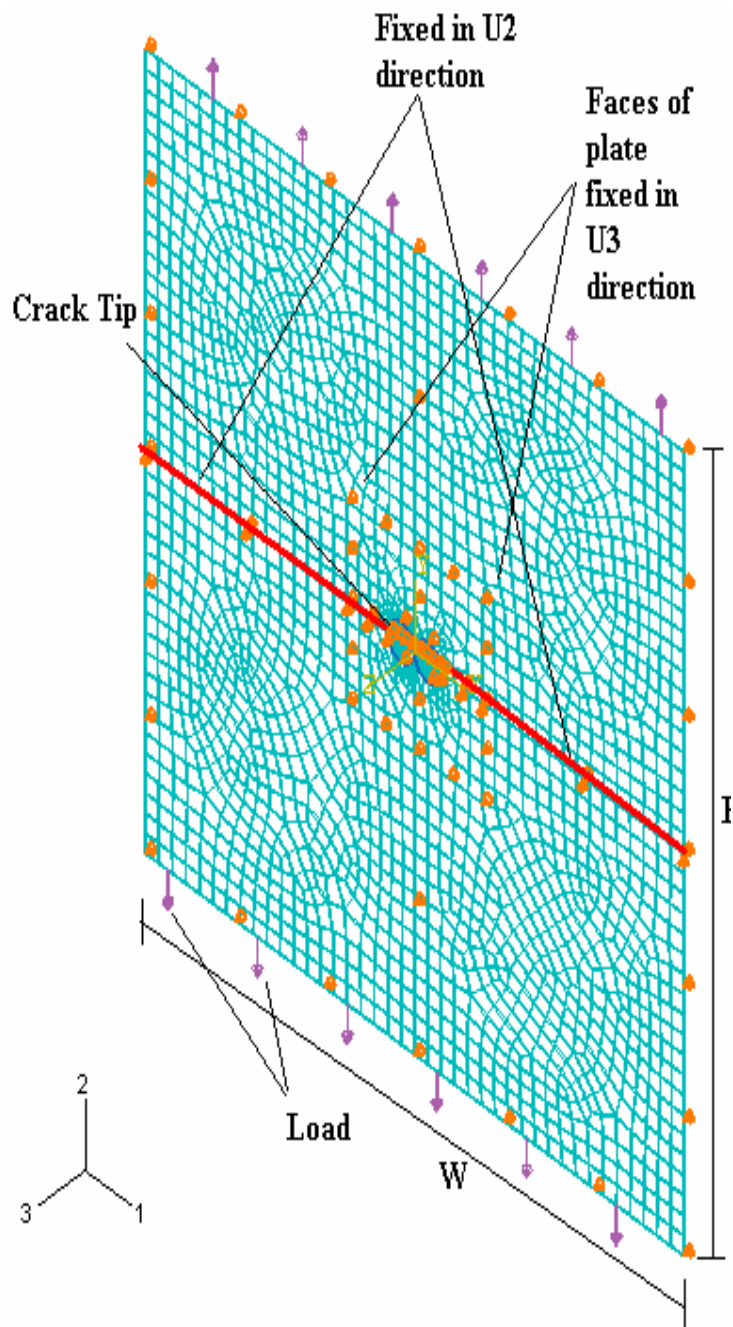


**Figure 4.2** ABAQUS mesh and model of the problem.

In ABAQUS software, model is created; boundary conditions and applied load are shown in Figure 4.2.

**Table 4.1** Dimensions and mechanical properties of the center through crack model

Dimensions and Properties	Values
Width of the plate, $w$	400 mm
Height of the plate, $h$	400 mm
Thickness of the plate, $t$	1 mm
Crack length of the plate, $a$	10 mm
Load on the plate in tension, $\sigma$	1 MPa
Young's modulus, $E$	13000 MPa
Poisson's ratio, $\nu$	0.15

Analytical solution for stress intensity factor in Mode I for this example is given in Equation 4.1. The Equation 4.1 was driven by Pilkey (1994).

$$K_I = \sigma \sqrt{\pi a} \times F_1(\alpha) \quad (4.1)$$

Correction factor is :

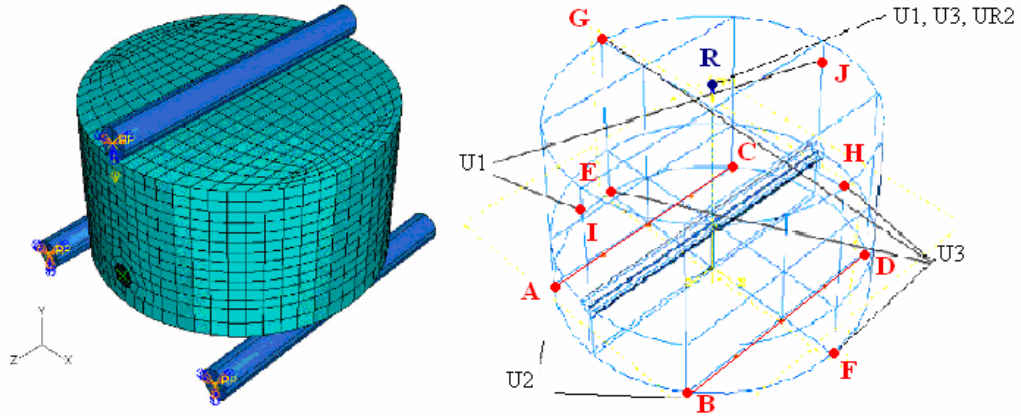
$$\alpha = \frac{a}{w}$$
$$F_1(\alpha) = (1 - 0.1\alpha^2 + 0.96\alpha^4) \sqrt{1/\cos(\pi\alpha)} \quad (4.2)$$

By using this analytical solution is found as 5.605 MPa $\sqrt{m}$  while the numerical computation yields 5.611 MPa $\sqrt{m}$  for the stress intensity factor. Percentage difference is around 0.12 %.

This means that ABAQUS numerical model generates a very close results compared to the analytical solution. ABAQUS can be comfortably used for the computations throughout this thesis work.

#### 4.4.1 Boundary Condition Verification

A new boundary condition system is used in this modelling work. So, for verification of this results are compared with the work of Alkılıçgil, 2006.



(a) Boundary conditions of Alkılıçgil (2006)

(b) Boundary condition entry location of the specimen model in this work

**Figure 4.3** Boundary conditions of verification

Alkılıçgil uses rigid roller supports and their rotations ( $R_x$ ,  $R_y$  and  $R_z$ ) are kept fixed in all directions. Loading in this work is applied to the rollers by using reference loading points above. In this work, boundary conditions are applied to the points and lines. Along the line AC and BD, displacement component along y ( $U_2$ ) is fixed. At points E, F, G and H, displacement component along Z ( $U_3$ ) is fixed, for points I and J, displacement component along x ( $U_1$ ) is fixed. And at point R (reference point) displacement components along x ( $U_1$ ), z ( $U_3$ ) and y rotation ( $U_{R2}$ ) are fixed, (Figure 4.3).

After running problem with new boundary conditions in ABAQUS, results show that new boundary conditions also give the same  $Y_I$  results as in Alkılıçgil, 2006.  $Y_I$  is found as 2.86.

## **4.5 Stress Intensity Factor Computation for SNDB**

Stress intensity factors computations are done with abaqus for SNDB technique (Figure 4.3). Specimen geometry was changed by using different thickness values (B) and span lengths (S/R).

### **4.5.1 Geometry and Boundary Conditions**

Diameter for SNDB specimens were 75 mm. Notch length was kept constant ( $a \approx 10$  mm) throughout the computations. Different thickness values (27, 37, 47, 67 mm) and various span lengths (45, 52.5, 60 and 67.5 mm) were tried to study the effect of B and S/R on stress intensity factor, respectively. Model is shown in Figure 4.4.

R: Radius of the specimen (mm)

D: Diameter of the specimen (mm)

a: Notch length (mm)

S: Span length (mm)

B: Height of the specimen (mm)

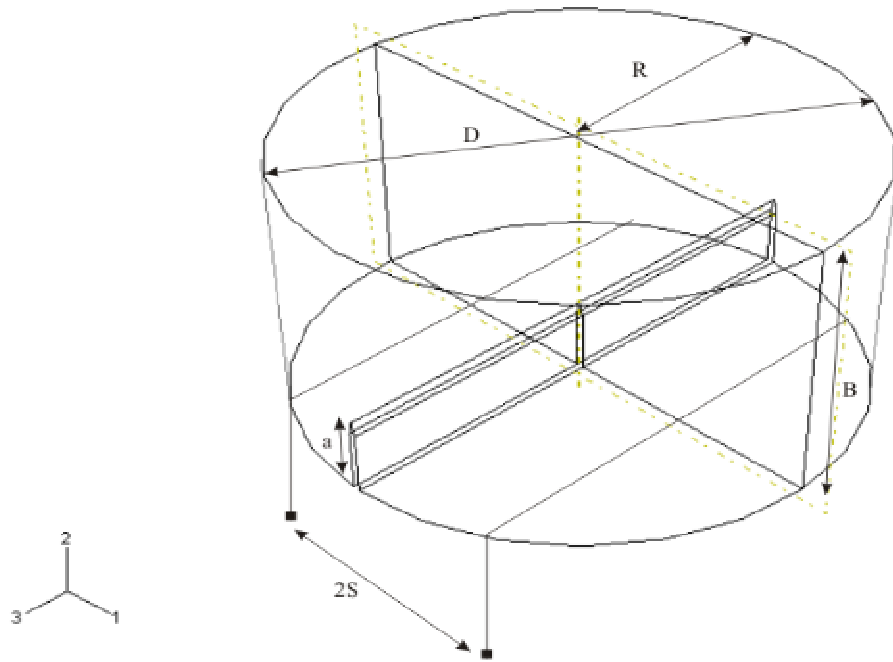


Figure 4.4 SNDB geometry

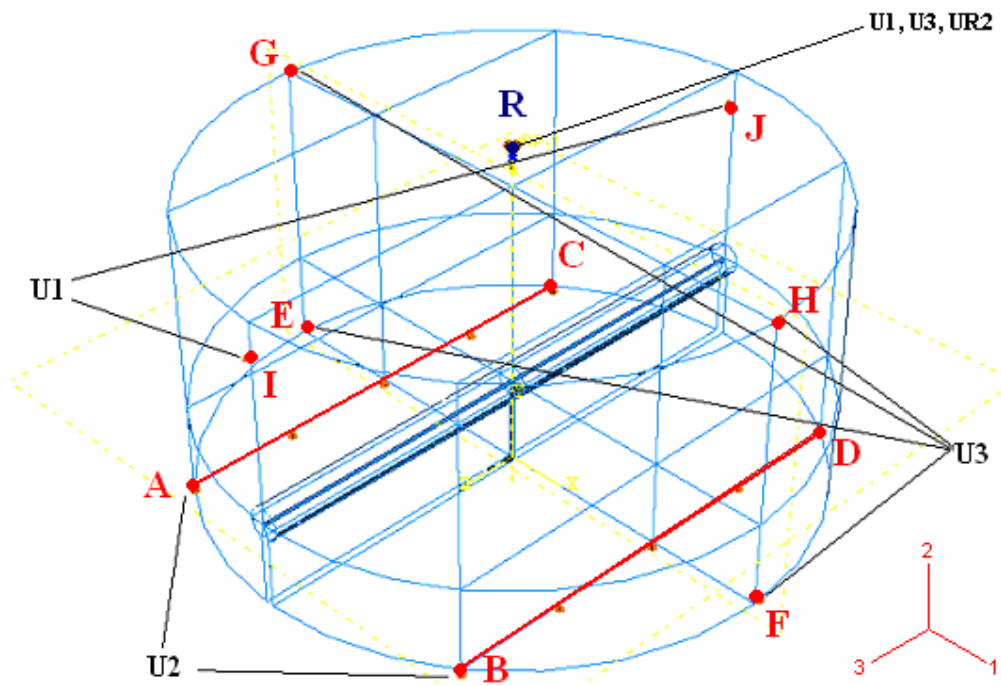
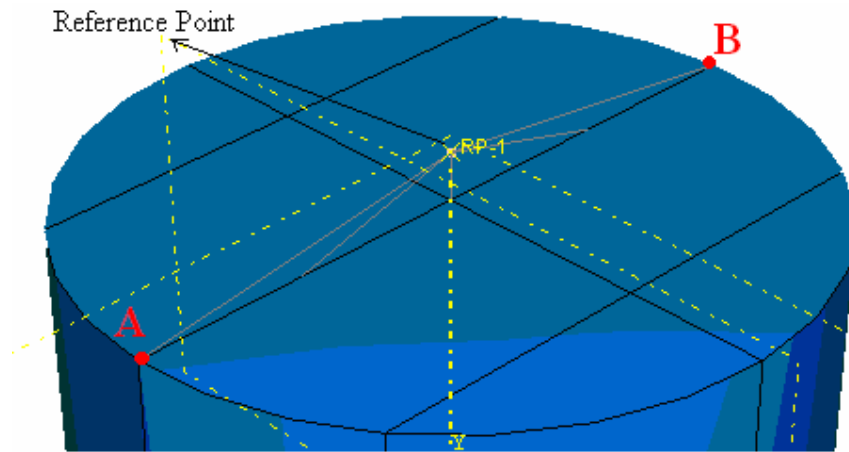
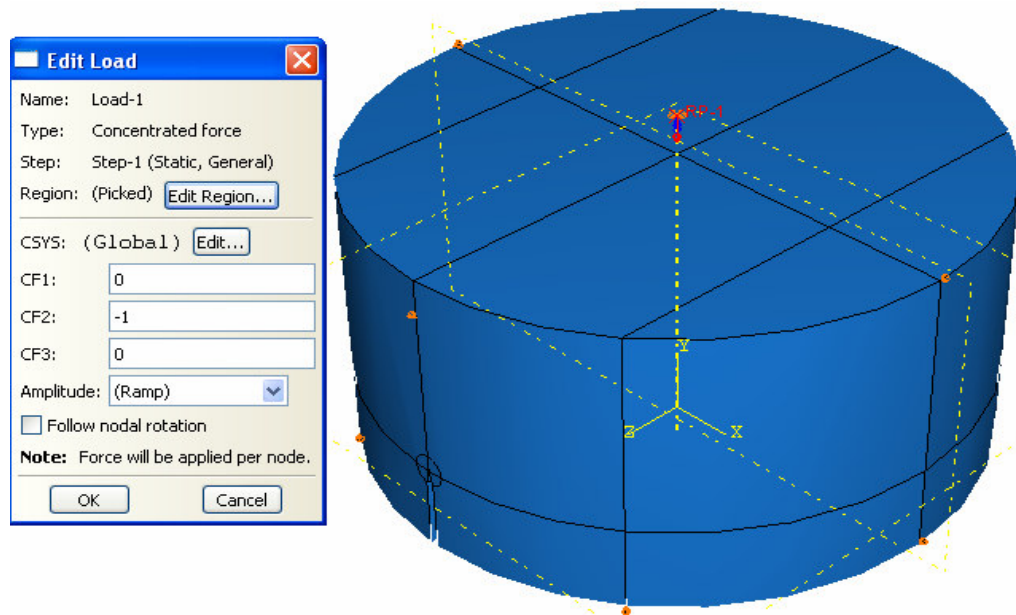


Figure 4.5 Boundary conditions

Along the lines AC and BD, displacement component along y ( $U_2$ ) is fixed. At points E, F, G and H, displacement component along Z ( $U_3$ ) is fixed, for points I and J, displacement component along x ( $U_1$ ) is fixed. And at point R (reference point) displacement components along x ( $U_1$ ),z ( $U_3$ ) and y rotation ( $U_{R2}$ ) are fixed, (Figure 4.5). Reference point is constraint to the AB line, (Figure 4.6). A unit negative vertical load ( $F_y = -1$  N) is applied to the AB line through the Reference Point-1, (Figure 4.7).



**Figure 4.6** Reference point constraint



**Figure 4.7** Applied Load

Crack tip loading is supposed to be pure Mode I loading for SNDB specimen, crack extension direction is attached in the vertical direction to the front of the initial vertical notch, (Figure 4.8).

Because of swept meshing could not be used due to the curved nature of the surface of the SNDB specimen model, a ring of wedge shape elements could not be assigned to the crack front. As a result, wedge elements can not be created here, and the crack tip singularity is not included for the contour integral estimates. However, according to the ABAQUS manuals in most cases the singularity at the crack line can be ignored if the mesh is sufficiently refined to model the deformation around the crack tip or crack line and the resulting high strain gradients. Mesh is refined around the crack for better computation of stress intensity factor.

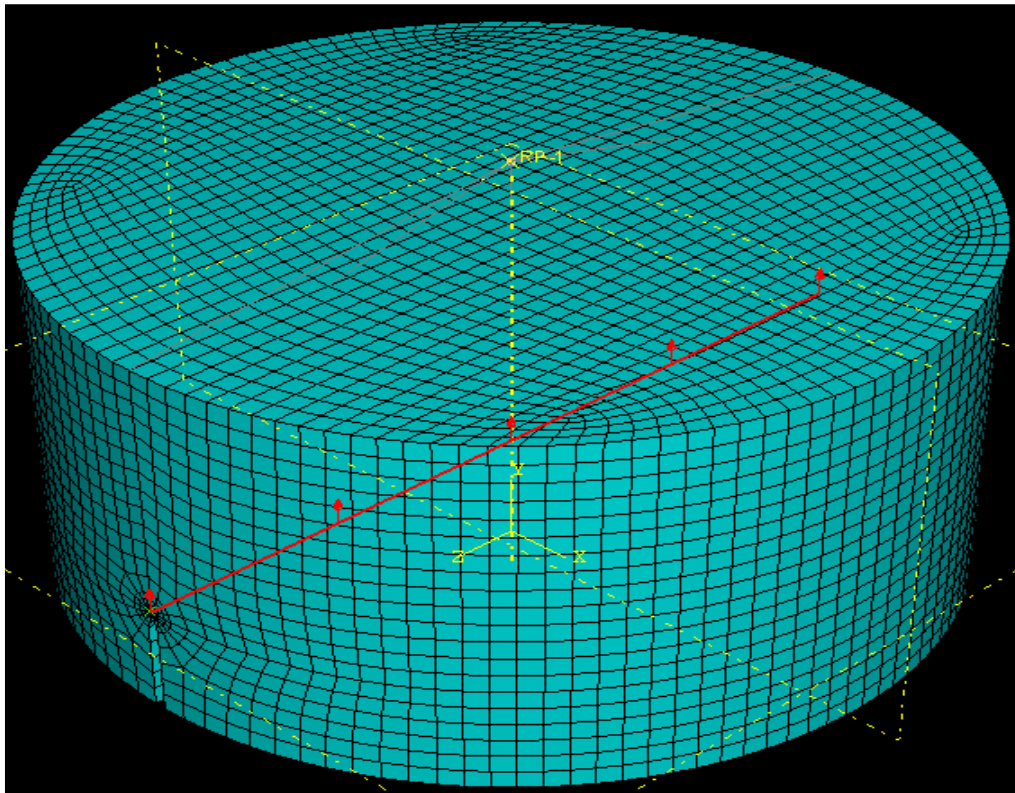


**Figure 4.8** Crack front and direction

### 4.5.2 Stress Intensity Factor Results for SNDB Specimens

Due to the beam type nature of the applied loading, Mode II stress intensity factor  $K_{II}$  is found to be very close to zero for all computations with ABAQUS. Therefore no entry for  $K_{II}$  is given in the results. In order to generalize the results and compare the  $K_I$  values to the other known geometries and loading conditions a normalized stress intensity factor is defined as:

$Y_I$  is calculated from Equation 4.3.

$$Y_I = \frac{K_I}{\sigma_0 \sqrt{\pi a}} \quad (4.3)$$

where,

$K_I$  = Mode I stress intensity factor computed by Abaqus

$$\sigma_0 = \frac{P}{2RB} \quad (4.4)$$

$P$  = applied load

$R$  = specimen radius

**Table 4.2** Normalized Mode I stress intensity factors for the SNDB specimens with  $D = 75$  mm

S/R	B/D				
	0.24	0.36	0.50	0.63	0.90
0.6	5.276	2.417	1.623	1.268	1.013
0.7	6.273	2.844	1.939	1.385	1.373
0.8		3.847	2.161	1.714	
0.9		3.899	2.474	1.969	

Grouping the specimens in each of the five B/D categories and averaging the stress intensity factors in each group, variation of normalized stress intensity factor versus specimen height B is shown in Figure 4.9. There is a sharp decrease in stress intensity factor till B/D = 0.4, then the rate decreases significantly. Stress intensity factor for the longer span (S/R=0.7) is about 16 % higher, meaning that notch tip is under higher tensile stress for longer spans.

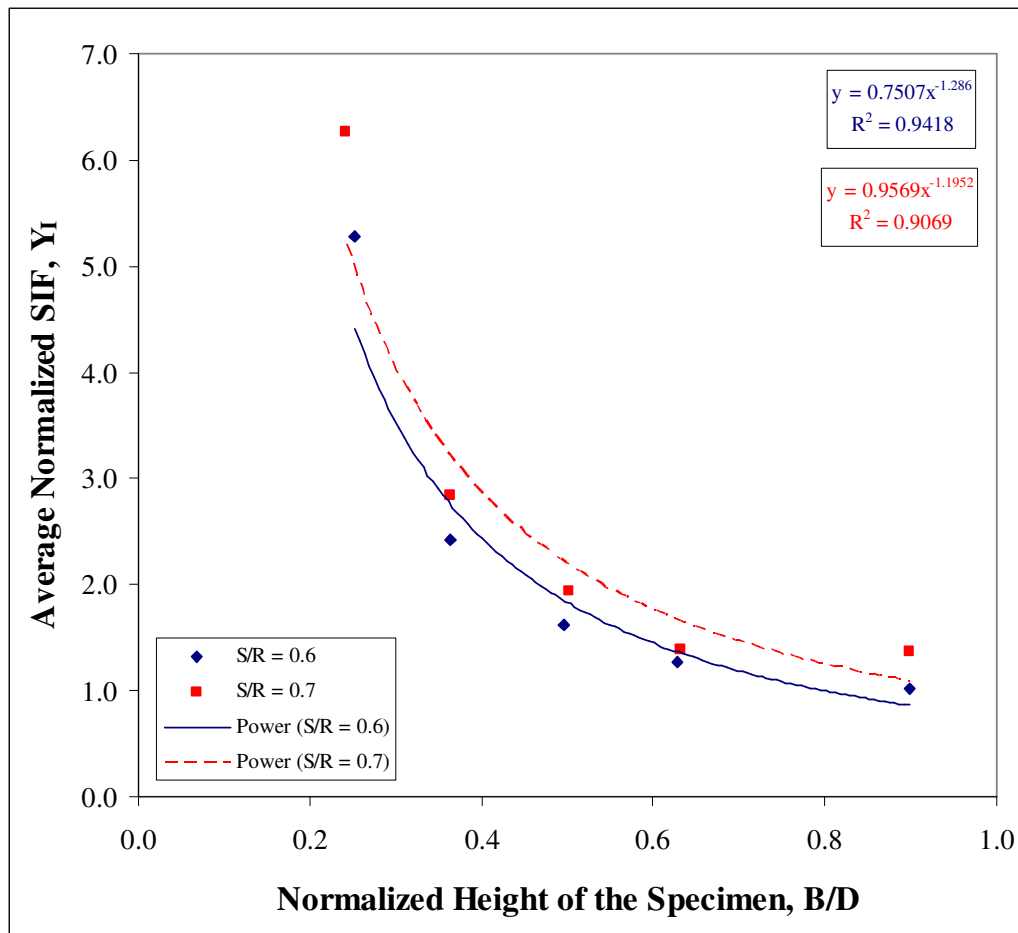


**Figure 4.9** Average normalized SIF versus normalized height of the andesite specimen, B/D

Stress intensity factors for changing spans ( $S/R=0.6, 0.7, 0.8$  and  $0.9$ ) were evaluated by grouping the specimens in their particular  $S/R$  and  $B/D$  category and averaging the results of the numerical computations. Average values of the normalized stress intensity factors were plotted against the changing span  $S/R$  ratios, (Figure 4.10).

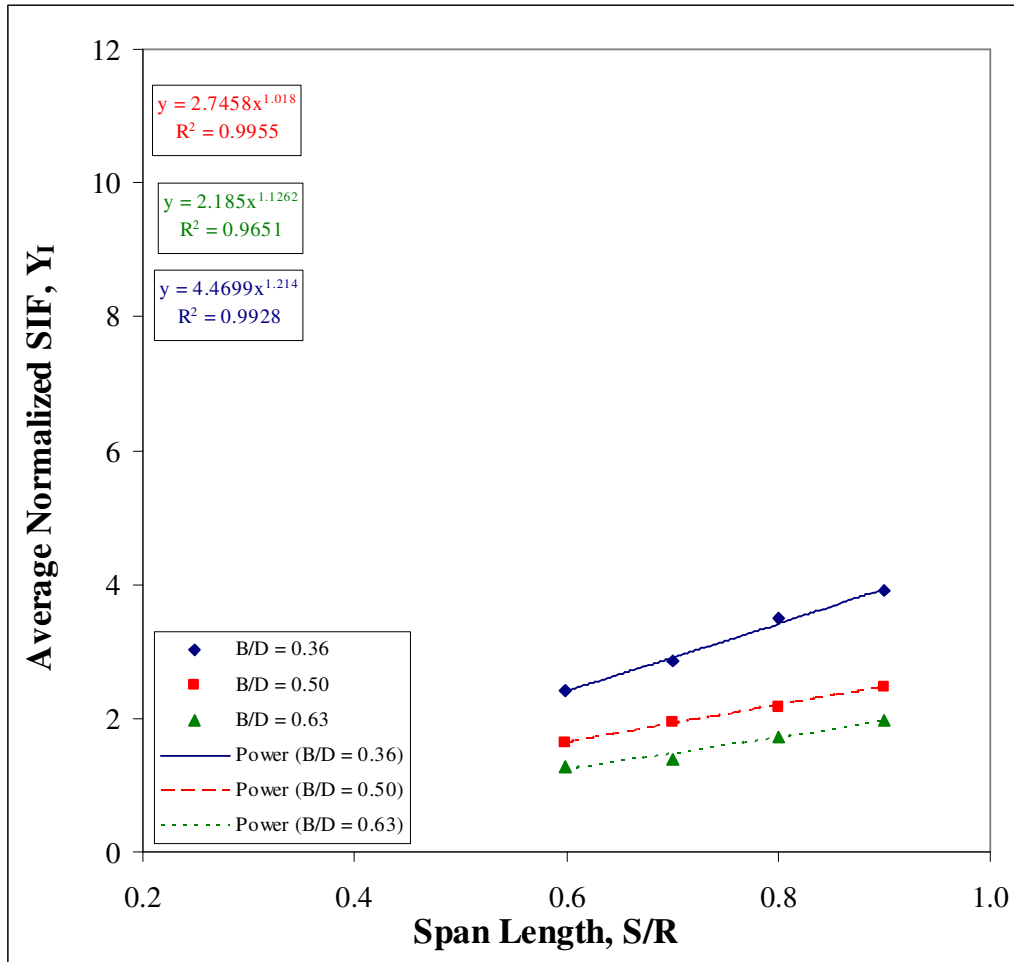


**Figure 4.10** Average normalized SIF versus loading span length for andesite

Stress intensity factor increases almost linearly with increasing  $S/R$  ratios, considering that power of  $x$  is around 1.1-1.2 for the fitted relations in Figure 4.10. Stress intensity factor, and thus notch tip tension is seen to be lower for  $B/D$  ratio of 0.63 compared to the  $B/D$  ratios of 0.50 and 0.36.

Variation of stress intensity factor versus specimen height B for marble is shown in the Figure 4.11. There is a sharp decrease in stress intensity factor up to  $B/D = 0.45$  then the rate decreases significantly.

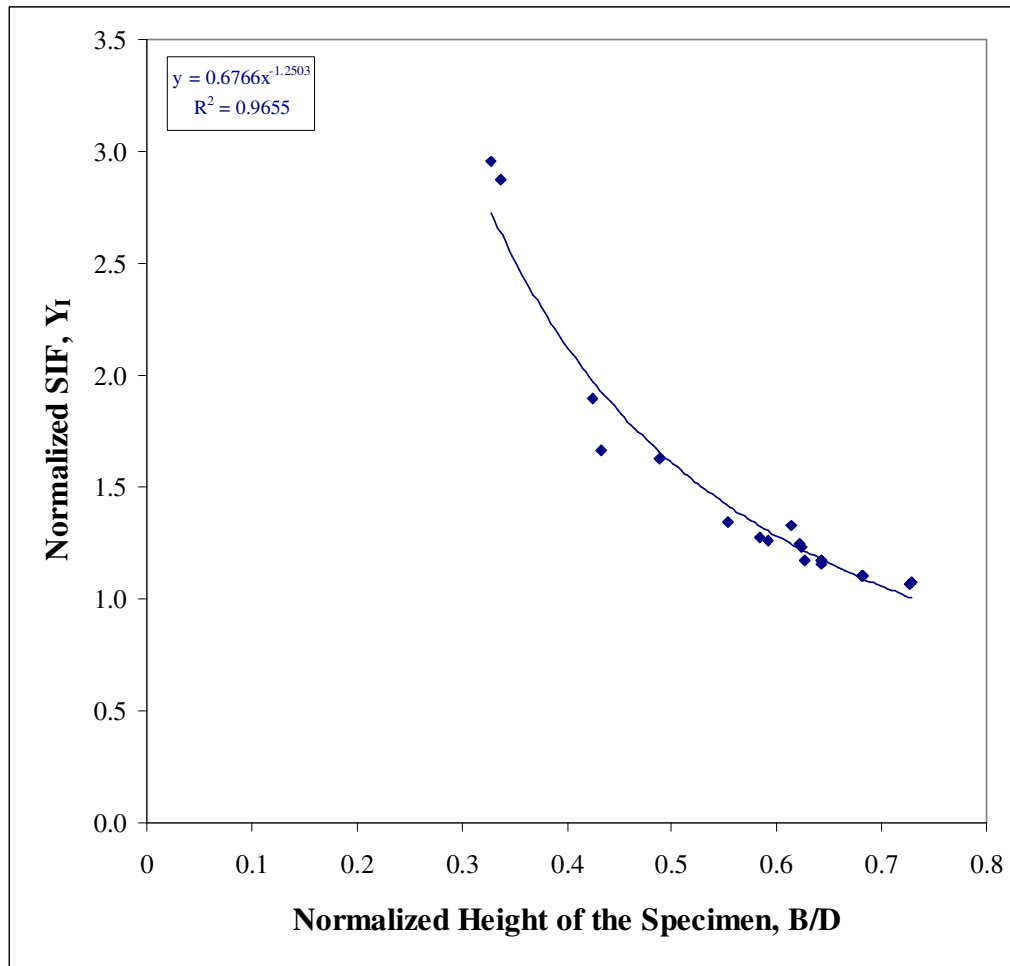


**Figure 4.11** Normalized SIF versus normalized height for the marble specimen

## 4.6 Stress Intensity Factor Change With Specimen Diameter

In the previous works, researchers usually carried out the stress intensity factor computations and fracture testing for a specific specimen diameter. For example Lim (1994) provided the relations of the stress intensity factors for 100 mm SCB specimens, Alkılıçgil (2006) presented the results for 100 mm SCB and SNDB specimens.

To see the effect of specimen diameter on the stress intensity factor ABAQUS models were developed for specimen diameters ranging from 42 to 125 mm. Stress intensity factors were computed for SNDB ( $S/R=0.7$  and  $B/a=5$ ) specimens, and results were tabulated in table 4.5. Results were plotted in Figure 4.12 for SNDB specimens.

**Table 4.3** SIF change with diameter for SNDB specimens

Diameter (mm)	Normalized SIF ( $Y_I$ )
42	1.14
54	1.21
75	1.47
100	1.86
125	2.68

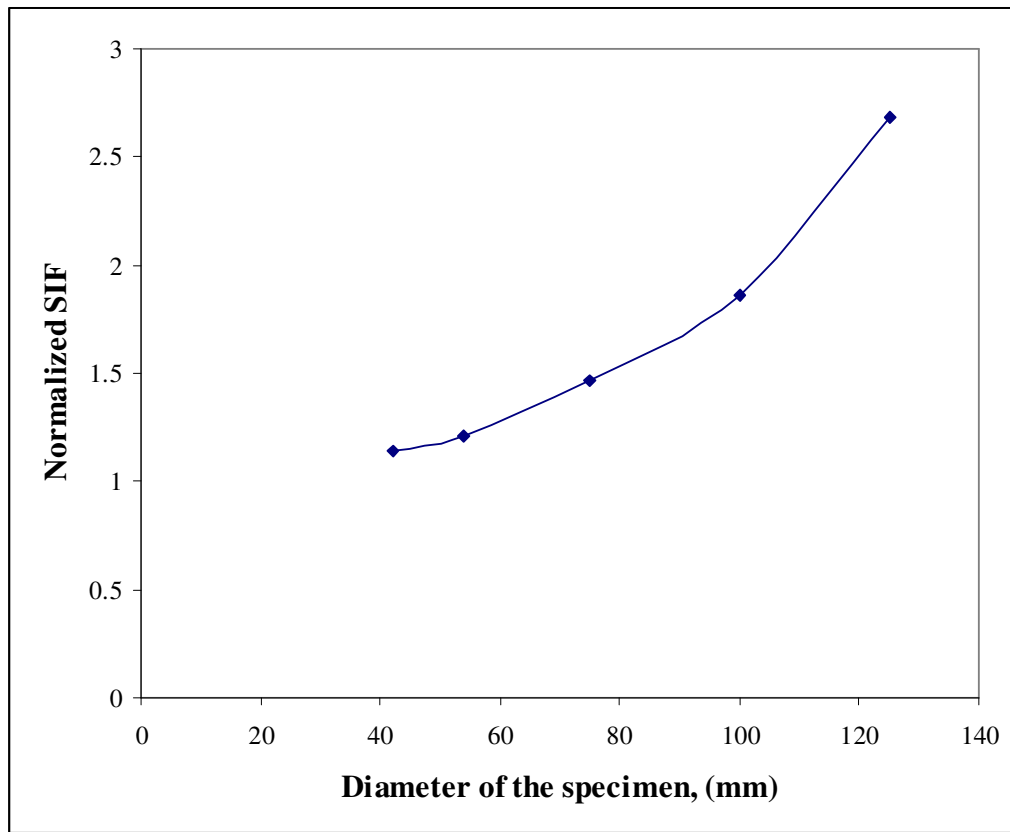


**Figure 4.12** Normalized SIF versus diameter of the specimen

As seen in the figures, stress intensity factor increases with increasing diameter for beam type specimens. Rate of increase is especially higher for specimens larger than 75 mm diameter. This means that larger specimens will have higher tensile stress fields around the notch front.

## **CHAPTER 5**

### **LABORATORY WORK**

In this section laboratory work is explained. Two types of rock were used in laboratory tests. The first rock type used in the experiments is Ankara Andesite which is taken from a quarry at the north side of Gölbaşı and the other rock type is white Afyon Marble. Disc type specimens are used in laboratory work which are called as Straight Notched Disc specimen under three-point Bending (SNDB).

Before fracture tests, to determine mechanical properties of the Ankara Andesite, and Afyon Marble uniaxial compressive strength (UCS) tests and tensile strength tests were carried out.

#### **5.1 Mechanical Properties of the Specimens**

##### **5.1.1 Ankara Andesite**

In order to determine the mechanical properties (Young's Modulus, Poison Ratio) of pink-gray coloured Ankara Andesite, uniaxial compressive strength (UCS) tests were done. During the experiments ISRM's (1979) suggested methods were employed. Five NX size specimens ( $54 \approx \text{mm}$ ) and  $L/D \geq 2$  were used in UCS tests. In the tests the MTS 815 Material Testing System was used. Two external LVDT transducers were used to measure the vertical displacement, vertical strain and circumferential extensometer was used to measure the circumferential displacement and strain, (Figure 5.1).



**Figure 5.1** UCS test: andesite specimen with circumferential and axial extensometer

As a result of 5 tests, average values of modulus of elasticity, Poisson's Ratio and UCS of the Ankara Andesite rock were found 21 GPa, 0.147 and 53.1 MPa respectively.

Indirect tensile tests were done to measure tensile strength of the Ankara Andesite in accordance with ISRM (1978). Four specimens were used in Brazilian tests and all of them were NX size samples ( $\approx 54$  mm). The MTS 815 Material Testing System was used for loading. Average tensile strength was calculated as 6.75 MPa, (Table 5.1).

**Table 5.1** Indirect tensile strength test data and results for Brazilian Test

Specimen Code	Diameter D (mm)	Length L (mm)	Tensile Strength $T_0$ (MPa)
Brazilian 1	52.79	26.41	6.53
Brazilian 2	53.12	26.56	6.86
Brazilian 3	52.70	28.77	6.38
Brazilian 4	52.83	26.80	7.24
Averages $\pm$ SD	$52.86 \pm 0.18$	$27.14 \pm 1.10$	$6.75 \pm 0.38$

### **5.1.2. Afyon Marble**

In order to determine the mechanical properties (Young's Modulus, Poisson Ratio) of Afyon marble, uniaxial compressive strength (UCS) tests were done. As a result of 5 tests, average modulus of elasticity of the Afyon marble was found as 14 GPa, the Poisson's Ratio was found as 0.184, (Figure 5.2).



**Figure 5.2** UCS test marble specimen with circumferential and axial extensometer

### **5.2 Preparation of Fracture Toughness Specimens**

Big blocks taken from quarry are taken to METU rock mechanics laboratory. These blocks are cut into smaller blocks with rotary saw in order to fit into the coring machine.

With coring machine 75 mm diameter cores were prepared. These blocks are then cut into approximately 30, 40, 50 and 70 mm specimens with Smartcut 1004 (Figure 5.3).



**Figure 5.3** Smartcut 1004

By using polishing machine, irregularities in the discs were removed. By the help of goniometer, center of the disc was marked by a line passing through the center of the upper and lower faces, (Figure 5.4).



**Figure 5.4** Goniometer

In order to cut the preliminary notch properly according to the desired dimensions, an apparatus was designed, (Figure 5.5). Notch length was adjusted with the help of a digital caliper, (Figure 5.5). During the travel of the holding fixture on the tracks, a notch with the desired length was cut through the specimen.



**Figure 5.5** Opening of notch in Smartcut 1004

After the notch is cut specimen dimensions are measured with a caliper. SNDB and SCB specimens are prepared by using this equipment for both marble and andesite rocks.

Before starting the experiments each specimen is coded considering its test method and geometry, (Figure 5.6).

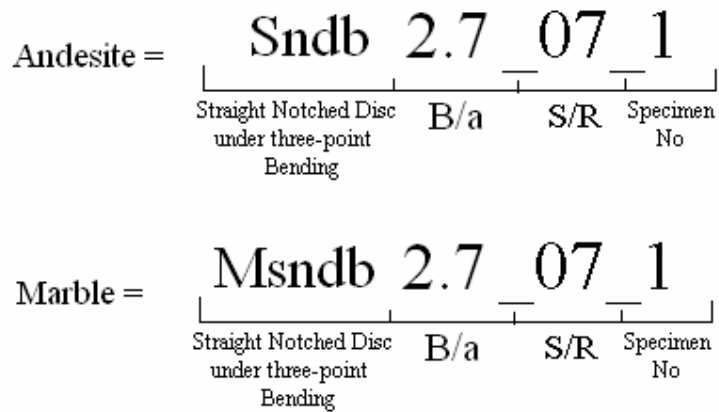


**Figure 5.6** Example SNDB code for andesite and marble respectively

In Figure 5.7, specimens before and after the tests can be seen.



(a) Before test

(b) After test

**Figure 5.7** Specimen and loading setup

### 5.3 Compressive Loading System

In experiments MTS 815, servo-controlled hydraulic testing machine was used for the application of compressive loads. MTS material test system is designed to accommodate a wide variety of standard material test. Typical system contains the following major components:

#### Electronic Products

- A MicroConsole and its associated AC and/or DC controllers
- A programming device (which maybe mounted in the MicroConsole, mounted in another chassis in the console, or externally connected)

#### Servo-hydraulic Devices

- A hydraulic actuator and its associated servovalves and transducers, mounted in load frame with maximum 2800 kN capacity
- A hydraulic power supply (HPS)

In operation of the system, the MicroConsole and its associated electronic products control the servohydraulic devices. The servohydraulic devices use hydraulic pressure supplied by the HPS to apply forces, displacement and/or strain to specimen, (MTS System Catalog, 1992).

#### 5.4 Data Acquisition System

A 16-bit 200kHz IOTech Daqbook/2000 series data acquisition system was used for data processing. DBK 80 device attached to the system is a low-noise, high-speed, unity-gain multiplexer card that provides 16 channels of differential voltage input. Load signal sent by the MTS external load cell of 500 kN capacity was processed and transferred to the PC by this module. Signals of the strain gage type displacement transducers were processed and transferred to the PC by DBK 43A module, (Figure 5.8).



**Figure 5.8** DBK80 Analog Multiplexer, DBK43 and DBK43A strain-gage cards

DaqView, which is a 32-bit Windows-based data acquisition program, is used to operate DBK cards and modules.

DaqView program takes the data as the tests go on. The data we take for our experiments include MTS load, and displacements of two displacement transducers mounted on the moving loading platen and crack opening displacement, (Figure 5.9).

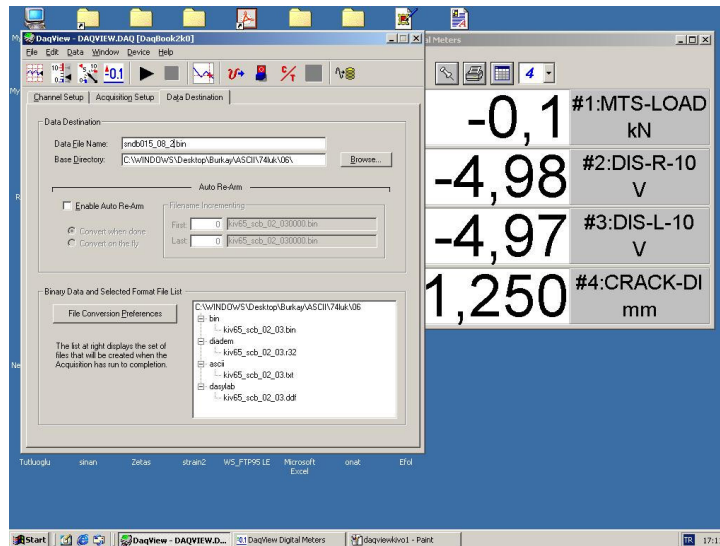


**Figure 5.9** DaqView program window and load and displacement readings

After data acquisition started, the “Run Button” was turned on the MicroConsole and “Direct Module”, “Run Enable” and “Program 4” were selected on Micro Profiler. Program 4 is programmed to move the loading piston in a displacement controlled way with a rate of 0.005 mm/sec. After data acquisition output is completed, the data is exported to an Excel file and required graphs were plotted.

## 5.5 SNDB Specimens

The loading fixtures and experimental setup are shown in Figure 5.10 for a typical SNDB specimen under three point bending. 10 mm diameter steel rollers apply the bending load to the specimen. Two linear displacement transducers are mounted on the bottom loading platen to keep a record of load-displacement behaviour.

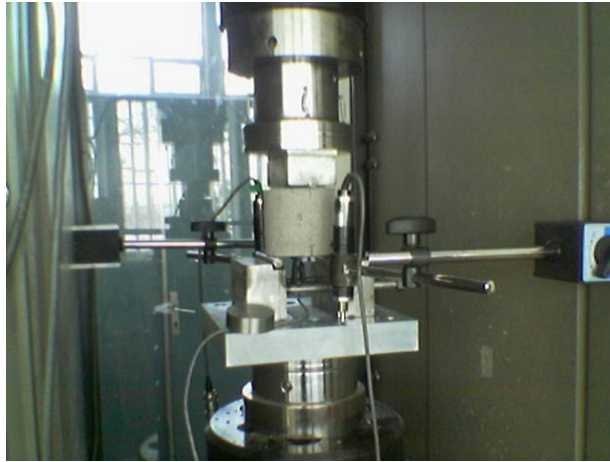
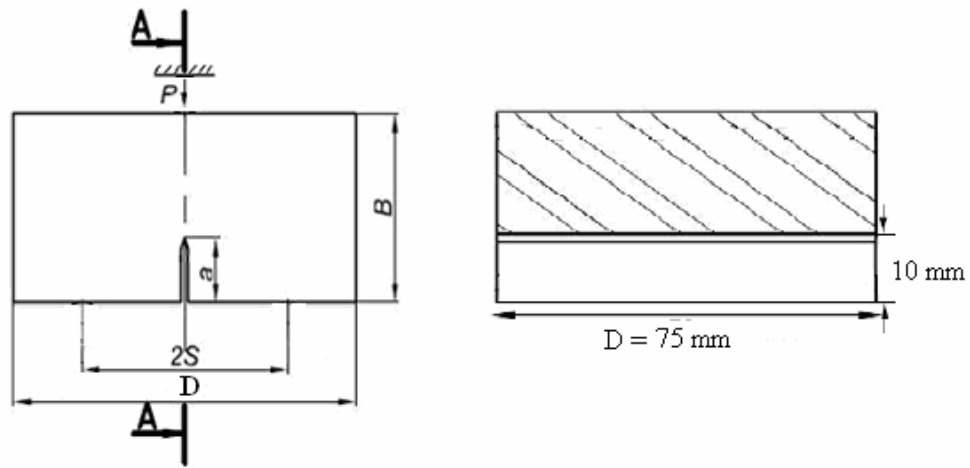


**Figure 5.10** SNDB specimen with steel rollers before the experiment

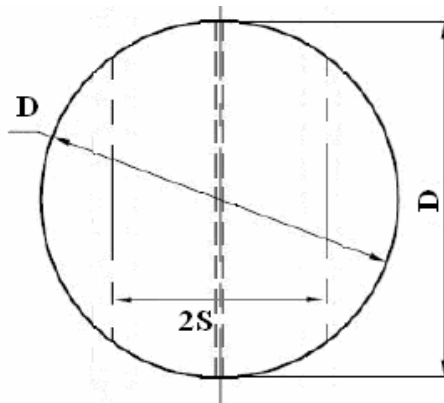
During the specimen preparation little variations of the dimensions were unavoidable in the critical geometrical parameters. In order to take into account the effect of dimensional differences on the stress intensity factors and fracture toughness, each specimen was modeled with its own dimensions in the computer models. When taking dimensions with a digital caliper, all front and back side dimensions were noted separately. Dimensions in the tables are the average values of the front-side and the back-side of the specimens.

Diameters of the disc specimens are approximately 75 mm. Thickness of the specimens were changed from 16 mm to 70 mm. Notch length kept constant for all specimens which is approximately 10 mm. Specimen geometry is illustrated in Figure 5.11.



(a) SNDB side view

(b) SNDB A-A cross section



(c) SNDB top view

**Figure 5.11** SNDB specimen geometry

The geometrical parameters related to the SNDB specimens are:

$B$  = Thickness or height of the specimen, (mm),

$D$  = Diameter of the specimen, (mm),  $2S$  = Span length, (mm),

$R$  = Radius of the specimen, (mm),  $a$  = Notch length, (mm),

A typical table illustrating the specimen dimensions for a series of tests is included in Table 5.2. Rest of the tables giving the specimen dimensions are presented in Appendix A.

**Table 5.2** Average Dimensions of  $S/R=0.6$  SNDB Specimens

Specimen Code	Notch length a (mm)	Diameter D (mm)	Radius R (mm)	Specimen Height B (mm)	Span length S (mm)	B/D	B/a	S/R
Sndb2.7_06	10.00	74.84	37.42	27.13	22.45	0.36	2.71	0.6
Sndb3.7_06	10.00	74.68	37.34	37.07	22.41	0.50	3.37	0.6
Sndb4.7_06	10.00	74.95	37.47	47.07	22.49	0.63	4.71	0.6
Sndb6.7_06	10.00	74.76	37.38	67.11	22.43	0.90	6.71	0.6

### 5.5.1 Span Length Analysis for Andesite

In the investigation of effect of loading span on the fracture toughness experiments with four different  $S/R$  ratios were conducted. These are  $S/R= 0.6, 0.7, 0.8$  and  $0.9$ . The dimensions of the specimens are given in Appendix A.

### 5.5.2 Specimen Height Analysis of Andesite

First analysis for SNDB type specimens is the investigation of the effect of andesite specimen height (B) on the fracture toughness. Five different specimen heights were used in the experiments (18, 27, 37, 47 and 67 mm). All of these specimens had the same notch length approximately 10 mm. Dimensions of all specimens can be seen in Appendix A.

### 5.5.3 Specimen Height Analysis of Marble

Last analysis for SNDB type specimens is the investigation of the effect of marble specimen height (B) on the fracture toughness. Five different specimen heights were used in the experiments (25, 32, 46, 48 and 54 mm). All of these specimens had the same notch length of approximately 10 mm. Dimensions of the marble specimens can be seen in Appendix A.

## CHAPTER 6

### RESULTS & DISCUSSIONS

Using the values in the dimension tables, specimens were modelled individually in ABAQUS.  $K_I$  values taken from ABAQUS are used to determine the normalized stress intensity factor ( $Y_I$ ).  $Y_I$  is used to calculate the fracture toughness. By using load-displacement data the maximum critical load and maximum vertical displacement values were determined. By the help of the normalized stress intensity factor and the maximum critical loads, fracture toughness were determined. Effect of different testing parameters on fracture toughness of Ankara andesite and Afyon marble were investigated.

#### 6.1 Computation Technique for SNDB Specimens

Finite element modelling with ABAQUS gives us  $K_I$  and  $K_{II}$  values.  $K_I$  values are normalized to  $Y_I$  by using the equation 6.1.

$$\text{Normalized Stress Intensity Factor } (Y_I) = \frac{K_I}{\sigma_0 \sqrt{\pi a}} \quad (6.1)$$

where:

$K_I$  = Mode I stress intensity factor

$$\sigma_0 = \frac{P}{2RB}$$

$P$  = Applied load (When modelling with ABAQUS it is taken as 1N)

$R$  = Specimen radius

By using normalized stress intensity factors ( $Y_I$ ) fracture toughness values are calculated by using equation 6.2.

$$K_{IC} = Y_I \sigma_{CR} \sqrt{\pi a} \quad (6.2)$$

where:

$$\sigma_{cr} = \frac{P_{CR}}{2RB} \quad (6.3)$$

$P_{CR}$  = Load at fracture,

$R$  = Specimen radius,

A sample computation with :

R: 0.03742 m

B: 0.02713 m

$K_I$ : 210.701 Pa $\sqrt{m}$

a: 0.010 m

is illustrated below.  $K_I$  value is obtained from numerical modelling with ABAQUS.

Substituting the values to the Equation 6.1,  $Y_I$  is:

$$Y_I = \frac{210.701Pa\sqrt{m}}{\sigma_0 \sqrt{\pi} \times 0.010m}$$

Calculation of the  $\sigma_0$  as below:

$$\sigma_0 = \frac{1N}{2 \times 0.03742m \times 0.02713m}$$

$$\sigma_0 = 492.51 \text{ N/m}^2$$

By applying the  $\sigma_0$  value to the first Equation 6.5,  $Y_I$  is:

$$Y_I = \frac{210.701 \text{ Pa} \sqrt{m}}{492.51 \text{ N/m}^2 \sqrt{\pi \times 0.010 \text{ m}}}$$

$Y_I$  is found as 2.417 according to this calculation procedure. After that fracture toughness is calculated by using Equations 6.2 and 6.3.

$$\sigma_{CR} = \frac{P_{CR}}{2RB} = \frac{4.193 \text{ kN}}{2 \times 0.03742 \text{ m} \times 0.02713 \text{ m}} = 2065.1 \times 10^3 \text{ N/m}^2$$

Then, the fracture toughness is:

$$K_{IC} = Y_I \sigma_{CR} \sqrt{\pi a} = 2.417 \times 2065.1 \times 10^3 \text{ N/m}^2 \sqrt{\pi \times 0.010 \text{ m}}$$

$$K_{IC} = 883,47 \times 10^3 \text{ Pa} \sqrt{m}$$

$$K_{IC} = 0.883 \text{ MPa} \sqrt{m}$$

## 6.2 Results of Changing Span Analysis for Andesite SNDB Specimens

In three point bending tests of SNDB, the load at the bottom is applied by two rollers separated by a span  $S$ . In this analysis effect of  $S/R$  ratio on the fracture toughness was investigated. Four different span ratios (0.6, 0.7, 0.8 and 0.9) were employed in the experiments. Three different specimen  $B/D$ 's (0.36, 0.50 and 0.63) were used in these tests.

Example table summarizes the details of a typical test series with  $S/R=0.6$ . Rest of the tables giving the fracture toughness results are presented in Appendix B.

Table 6.1 gives the results of this investigations where:

$P_{CR}$ : Failure load, (kN),

$K_I$ : Mode I stress intensity factor calculated with ABAQUS, ( $Pa\sqrt{m}$ ),

$Y_I$ : Normalized stress intensity factor,

$K_{IC}$ : Fracture toughness, ( $MPa\sqrt{m}$ ),

**Table 6.1** Results of S/R=0.6 andesite specimens

Specimen Code	Failure Load $P_{CR}$ kN	SIF $K_I$ $Pa\sqrt{m}$	Normalized SIF $Y_I$	Fracture Toughness $K_{IC}$ $MPa\sqrt{m}$
Sndb1.8_06_1	0.59	705.00	4.95	0.414
Sndb1.8_06_2	1.17	697.00	5.49	0.813
Sndb1.8_06_3	0,94	698.52	5.38	0.655
Sndb2.7_06_1	3.46	210.70	2.42	0.724
Sndb2.7_06_2	3.54	210.70	2.42	0.755
Sndb3.7_06_1	8.48	109.05	1.62	0.919
Sndb3.7_06_2	8.85	109.05	1.62	0.965
Sndb4.7_06_1	15.00	63.63	1.27	0.954
Sndb4.7_06_2	19.10	63.63	1.27	1.214
Sndb4.7_06_3	17.50	63.63	1.27	1.111
Sndb4.7_06_4	16.9	63.63	1.27	1.077
Sndb5.2_06_1	30.44	43.24	0.98	1.316
Sndb5.6_06_1	28.13	44.77	1.07	1.079
Sndb6.7_06_1	35.00	35.74	1.01	1.247
Sndb6.7_06_2	30.40	35.74	1.01	1.084
Sndb6.7_06_3	33.10	35.74	1.01	1.179

Figure 6.1 shows the results of the all tests together with plots of  $K_{IC}$  versus  $S/R$  ratios for different  $B/D$  levels. The quality of the fits for  $S/R$  behaviour is very low for all  $B/D$  levels. According to the results changing span does not have any significant effect on fracture toughness.

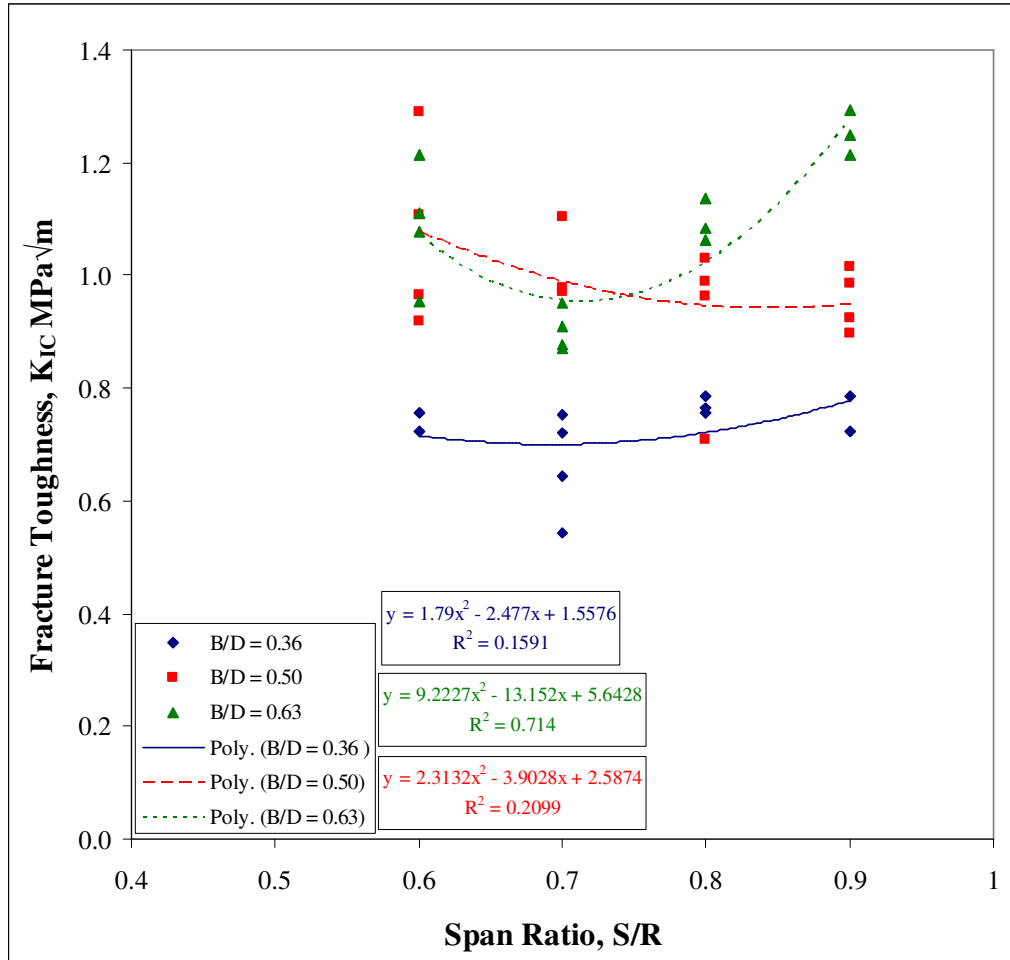


**Figure 6.1** Fracture toughness versus span ratio for andesite

It is seen from the figure that for the small specimen height case, that is  $B/D = 0.36$ , fracture toughness values are lower.

Averaging the results in their own groups and plotting fitted curves as in Figure 6.2, changing span does not have any affect on  $K_{IC}$ , since the curves show mixed trends with changing S/R ratios.

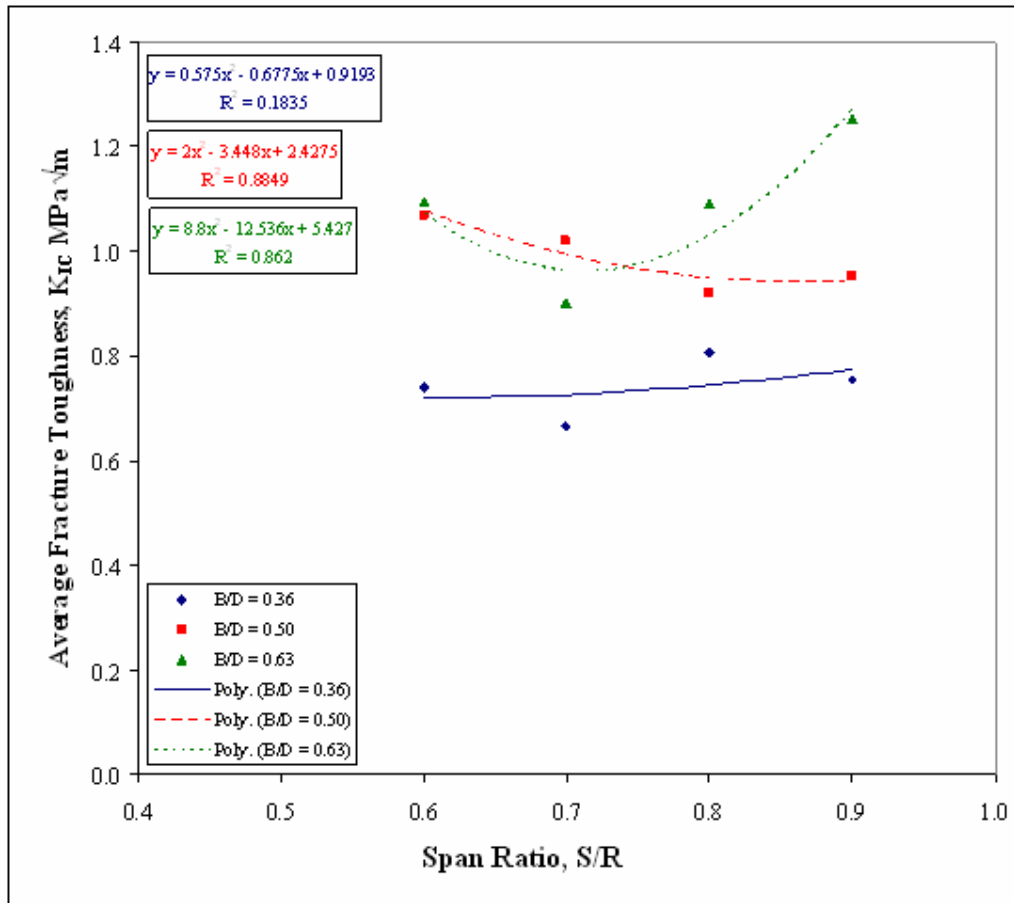


**Figure 6.2** Average fracture toughness versus span ratio for andesite

### 6.3 Results of Specimen Height Analysis of Andesite

First analysis for SNDB type specimens is the investigation of the effect of the height of the specimen on the fracture toughness. Five different specimen heights were used in the experiments ( $B = 18, 27, 37, 47$  and  $67$  mm). All of these specimens have the same notch length of approximately 10 mm. Two span ratios  $S/R = 0.6$  and  $=0.7$  were used for andesite specimens

For the span group  $S/R=0.6$  a total of 16 experiments were carried on SNDB type specimens with about 1-4 tests for same specimen height groups, (Table 6.1).

By carrying out some individual tests which were shown as single test in the tables points were tried to be added in identifying a trend of fracture toughness versus specimen height  $B$ .

Similarly for the span group of  $S/R=0.7$  a total of 18 experiments were conducted with again 1-4 tests for the same height group and some single points were added with additional tests to clarify the trend of fracture toughness with changing specimen height  $B$ , (Table 6.2).

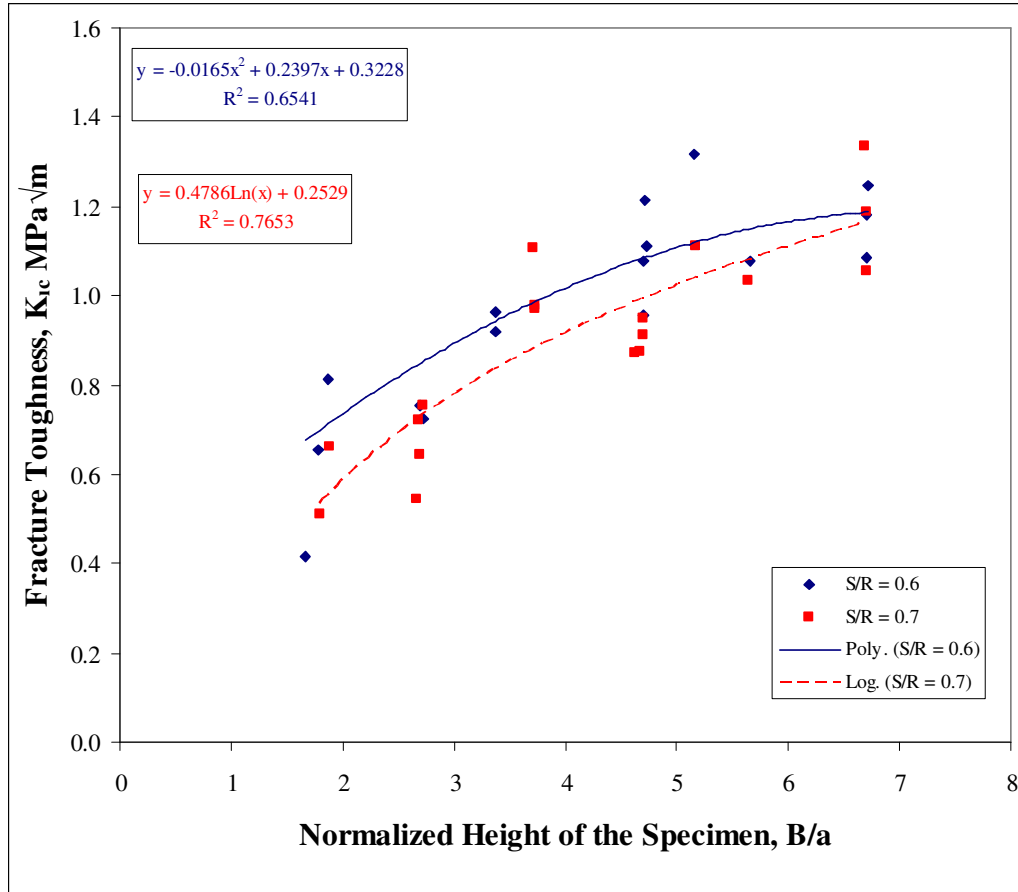
During the preparation of specimens, deviations in the specimen dimensions such as diameter and especially preliminary notch length were unavoidable due to mechanical difficulties and specimen heterogeneities. These variations were reported to effect stress intensity factor and fracture toughness computations, (Het, 2008). Therefore, in treating the results of height analysis and generating the plots of  $K_{IC}$  versus height, two alternatives were considered as  $K_{IC}$  versus  $B/D$  and  $B/a$

**Table 6.2** Results of S/R=0.7 andesite specimens

Specimen Code	Failure Load $P_{CR}$ kN	SIF $K_I$ $Pa\sqrt{m}$	Normalized SIF $Y_I$	Fracture Toughness $K_{IC}$ $MPa\sqrt{m}$
Sndb1.8_07_1	0.75	818.10	6.15	0.512
Sndb1.8_07_2	0.80	826.19	6.37	0.662
Sndb2.7_07_1	2.86	251.66	2.84	0.722
Sndb2.7_07_2	3.01	251.66	2.84	0.753
Sndb2.7_07_3	2.13	251.66	2.84	0.543
Sndb2.7_07_4	2.58	251.66	2.84	0.643
Sndb3.7_07_1	7.84	124.75	1.94	0.972
Sndb3.7_07_2	7.93	124.75	1.94	0.987
Sndb3.7_07_3	8.77	124.75	1.94	1.106
Sndb4.7_07_1	13.40	70.94	1.38	0.949
Sndb4.7_07_2	12.10	70.94	1.38	0.869
Sndb4.7_07_3	12.40	70.94	1.38	0.876
Sndb4.7_07_4	13.00	70.94	1.38	0.911
Sndb5.2_07_1	20.38	54.54	1.24	1.112
Sndb5.6_07_1	20.21	51.16	1.27	1.034
Sndb6.7_07_1	24.40	48.587	1.37	1.187
Sndb6.7_07_2	27.4	48.587	1.37	1.335
Sndb6.7_07_3	21.8	48.587	1.37	1.054

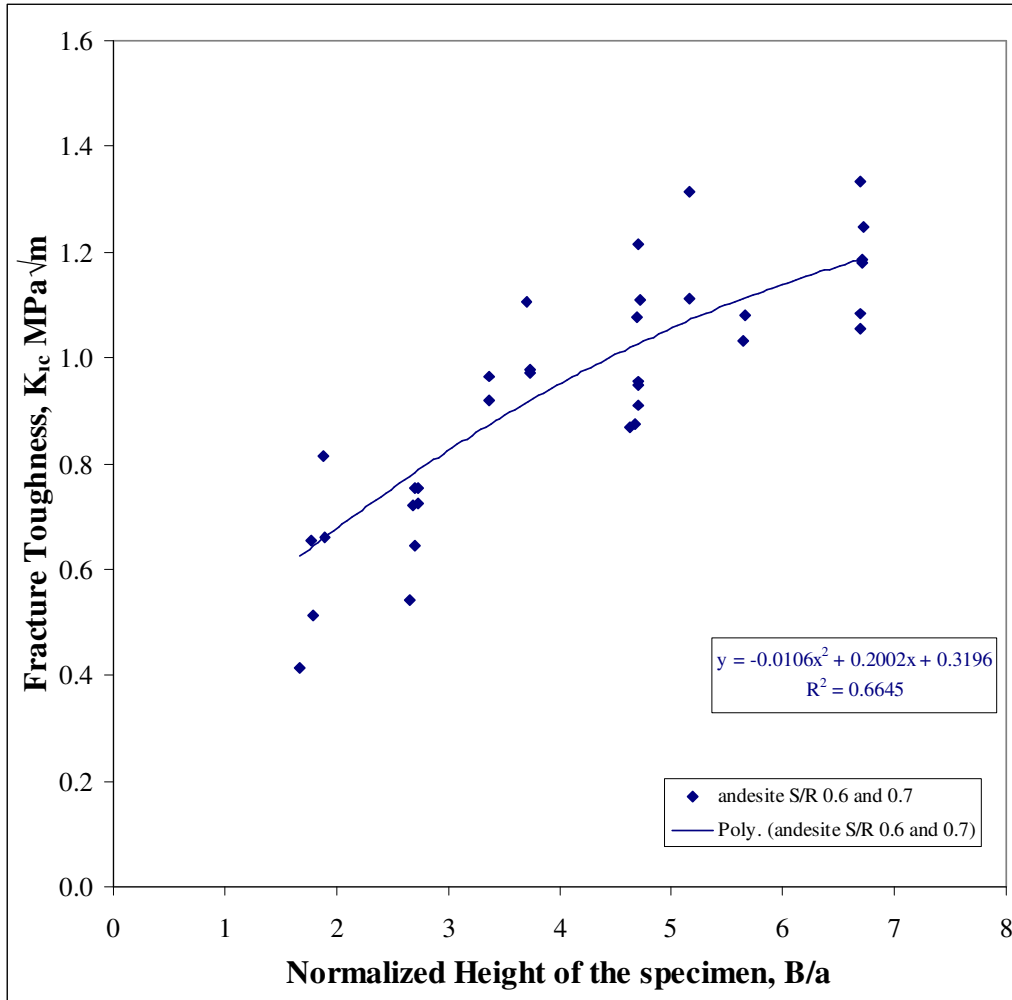
By using tables 6.1 and 6.2, fracture toughness values together for all B/a and S/R groups were plotted against the changing specimen height B/a in Figure 6.3. In this figure  $K_{IC}$  values versus B/a were treated statistically by fitting separate curves for each S/R group. With low  $R^2$  (around 0.65-0.76) values, quality of regression process is not very good. However with low B/a values, especially lower than B/a=3.0 fracture toughness values are clearly seen to be almost twice as much lower than values above B/a=3.0. Increasing trend in fracture toughness with B/a diminishes above B/a values approximately around 3.5 to 4.0, (Figure 6.3).

Having points within each other in the graphs for two different span groups, fracture toughness seems to be unaffected by changing loading span. On the other hand,  $K_{IC}$  values seem to be a little lower for longer span (S/R=0.7) than the shorter span case with S/R=0.6. This point has to be investigated further by increasing the number of tests and statistical quality of the regression analysis and fits.



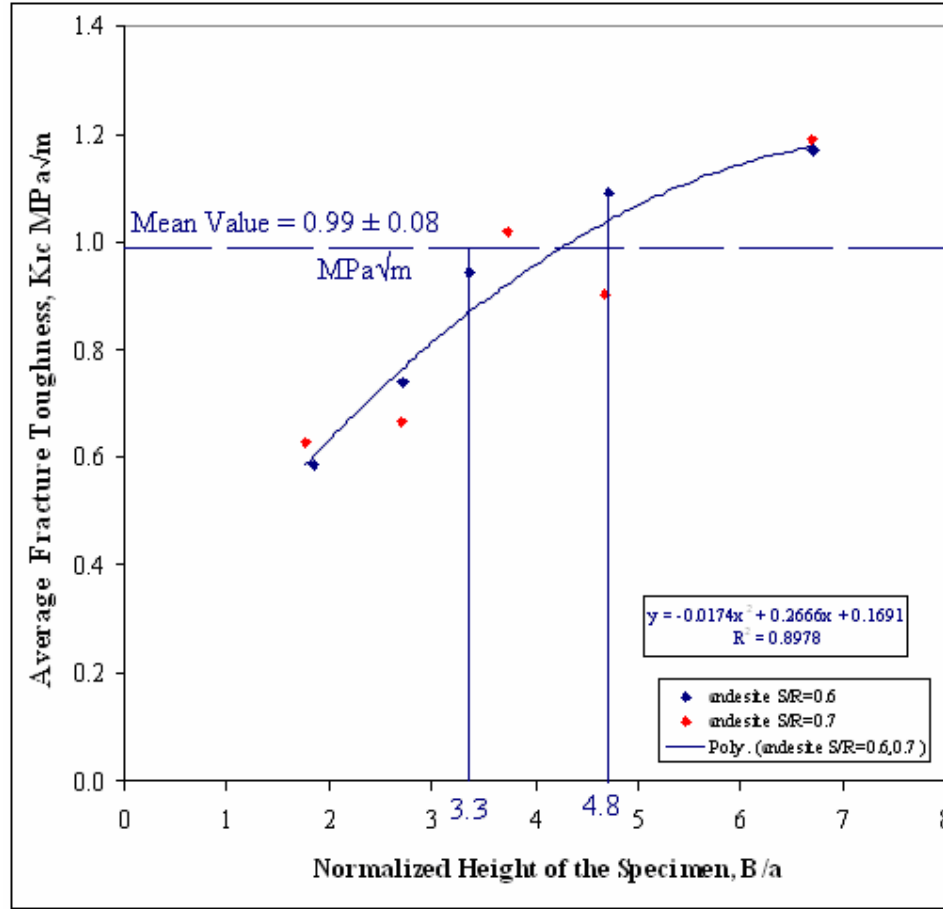
**Figure 6.3** Fracture toughness versus normalized height of the andesite specimen for different S/R ratios separately

Figure 6.4 shows a regression analysis and fit for all tests disregarding the effect of S/R ratio and treating all tests together for both S/R ratios. Statistical quality does not improve very much, possibly due to the brittleness and heterogeneous nature of the andesite samples. However, results are seen to scatter around  $K_{IC} = 1.0 \text{ MPa}\sqrt{\text{m}}$  for tests with B/a greater than 3.0, when results of tests with B/a greater than 3.0 are averaged for both S/R=0.6 and 0.7,  $K_{IC}$  value for andesite is found as  $0.99 \text{ MPa}\sqrt{\text{m}}$  which is very close to the value obtained in a similar work by Alkılıçgil (2006),  $0.93 \text{ MPa}\sqrt{\text{m}}$ .



**Figure 6.4** Fracture toughness versus normalized height of the andesite specimen

Grouping the same B/a specimens and averaging the results in their individual groups, the results are given in Figure 6.5. It is seen from the behaviour in this figure that a better fit is obtained and the fracture toughness shows a tendency to a value above 1 MPa $\sqrt{m}$ . If the fracture toughness values above B/a = 3.0 is averaged fracture toughness value is found as 1.08 MPa $\sqrt{m}$ . However,  $K_{IC}$  values only for B/a between 3.3 and 4.8, dont seem to change much and they show a tendency to a constant value of 0.99 MPa $\sqrt{m}$  when treated together, (Figure 6.5).



**Figure 6.5** Average fracture toughness of S/R = 0.6 and 0.7 andesite specimens

Averaging groups and combining the results for all S/R ratios good quality of fit and behaviour in Figure 6.6 indicates that fracture toughness increases with B/a, remaining almost constant between B/a= 3.3 and 4.8. After B/a= 4.8 there is again an increasing trend in K<sub>IC</sub>. The average value of B/a = 3.3 and 4.8 height levels is 0.99 MPa√m, which is very close to the value reported by Alkılıçgil (2006), 0.93 MPa√m for the andesite. Therefore, for the SNDB specimens in order to have valid fracture toughness results B/a ratio must be kept between 3.3 and 4.8.

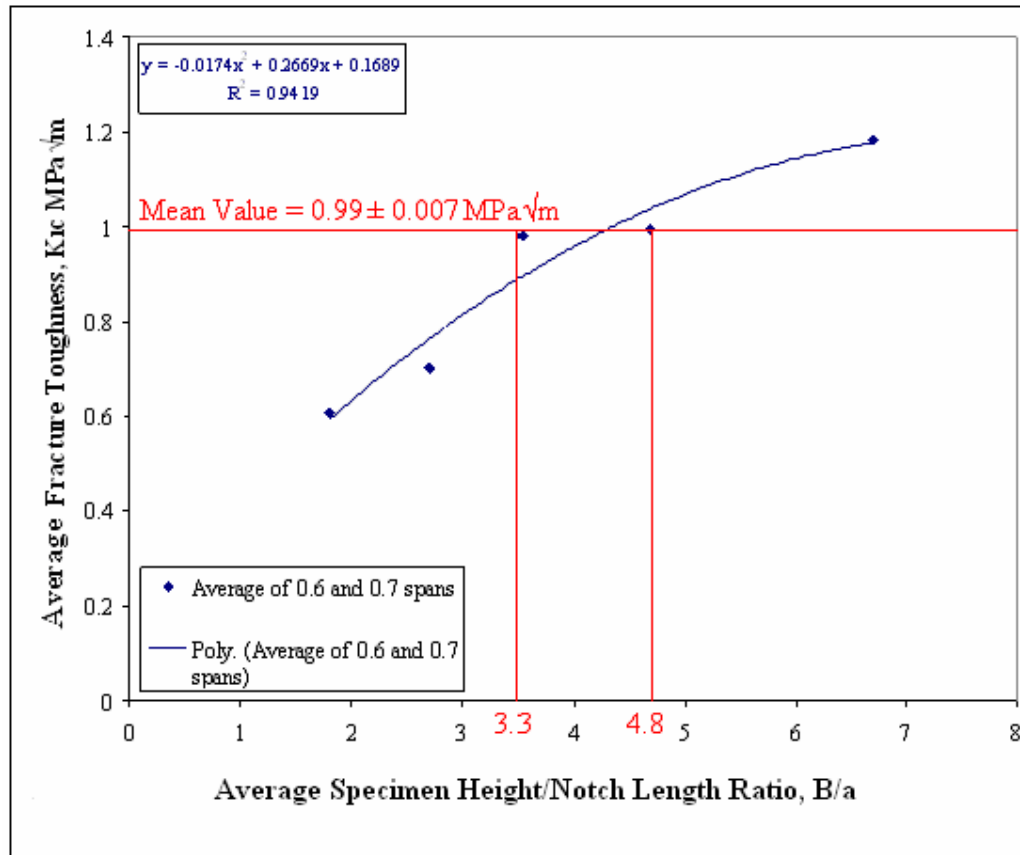


**Figure 6.6** Average fracture toughness versus average specimen height/notch length for all andesite specimen groups

By using tables 6.1 and 6.2, fracture toughness values together for all B/D and S/R groups were plotted against the changing specimen height/specimen diameter (B/D) ratio in Figure 6.7. In this figure  $K_{IC}$  versus B/D behaviour was treated statistically by fitting separate curves for each S/R group. Comparing the behaviour in Figure 6.7 to the fracture toughness versus B/a behaviour in Figure 6.3, it is seen that quality of fits are improved when treating the results with respect to the B/D ratios. This means that preparation and dimensions of the preliminary notch play an important role in the evaluation of fracture toughness. Variations in preliminary notch length cause a wider scatter in  $K_{IC}$  determinations.

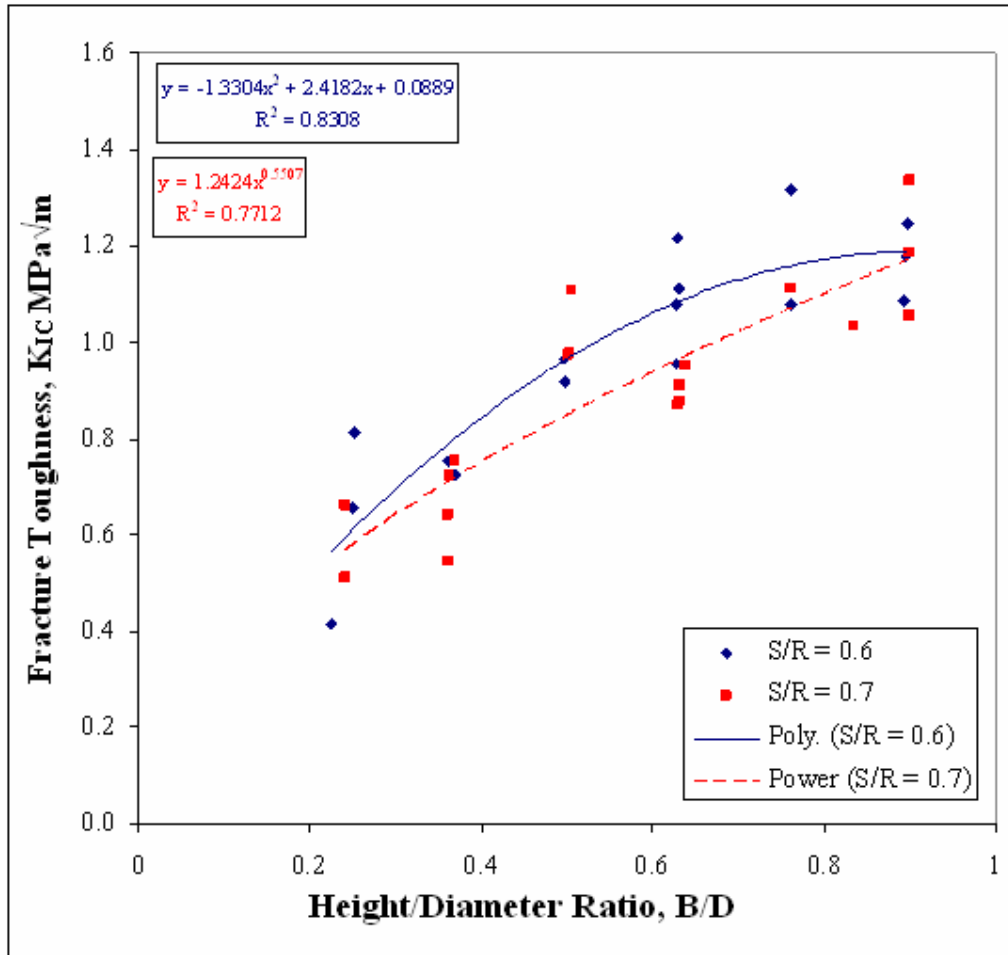


**Figure 6.7** Fracture toughness versus height/diameter ratio for all tests on andesite

Grouping the same B/D specimens and averaging the results in their individual groups, the results are given in Figure 6.8. It is seen from the behaviour in this figure that a better fit is obtained and the fracture toughness shows a tendency to a value above 1 MPa√m. K<sub>IC</sub> values for B/D between 0.49 and 0.64, don't change much, and they show a tendency to a constant value of 0.99 MPa√m when treated together, (Figure 6.8).

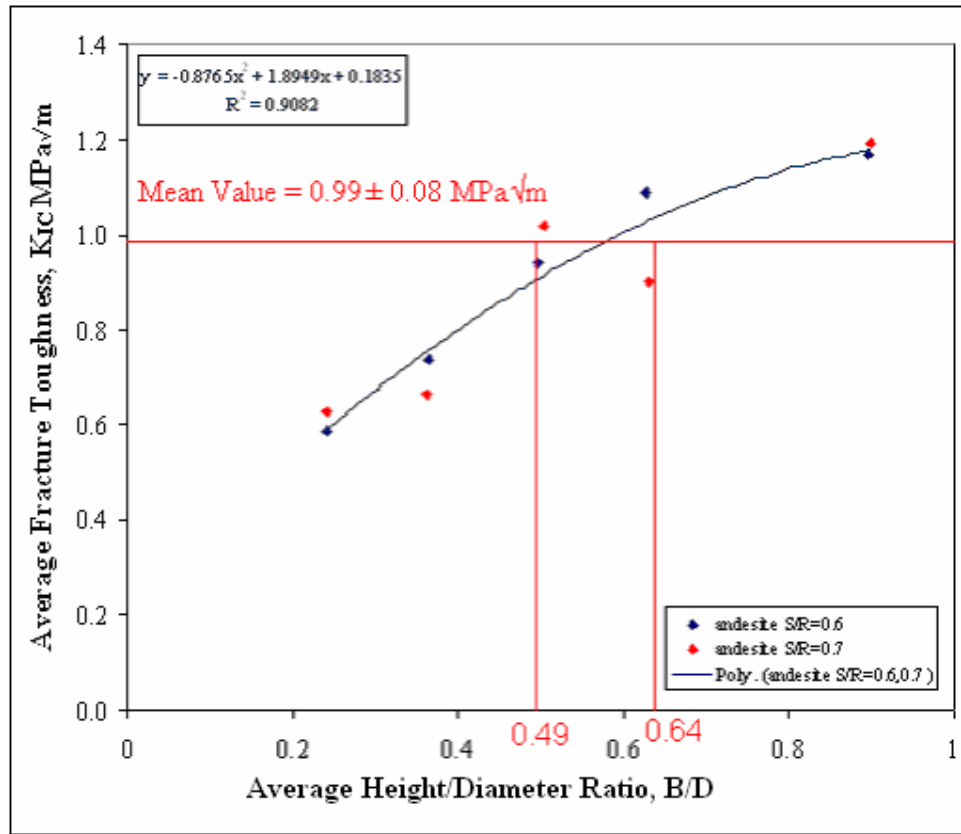


**Figure 6.8** Average fracture toughness versus average height/diameter ratio for andesite specimens with S/R = 0.6 and 0.7

Earlier it was found that S/R ratio doesn't have a significant effect on  $K_{IC}$ . Therefore, averaging groups and combining the results for all S/R ratios good quality of fit and behaviour in Figure 6.9 indicate that fracture toughness increases with B/D, remaining almost constant between B/D= 0.49 and 0.64. After B/D= 0.64 there is again an increasing trend in  $K_{IC}$ . The average value of B/D = 0.49 and 0.64 height levels is 0.99. Therefore, for the SNDB specimens, in order to have valid fracture toughness results B/D ratio must be kept between 0.49 and 0.64.

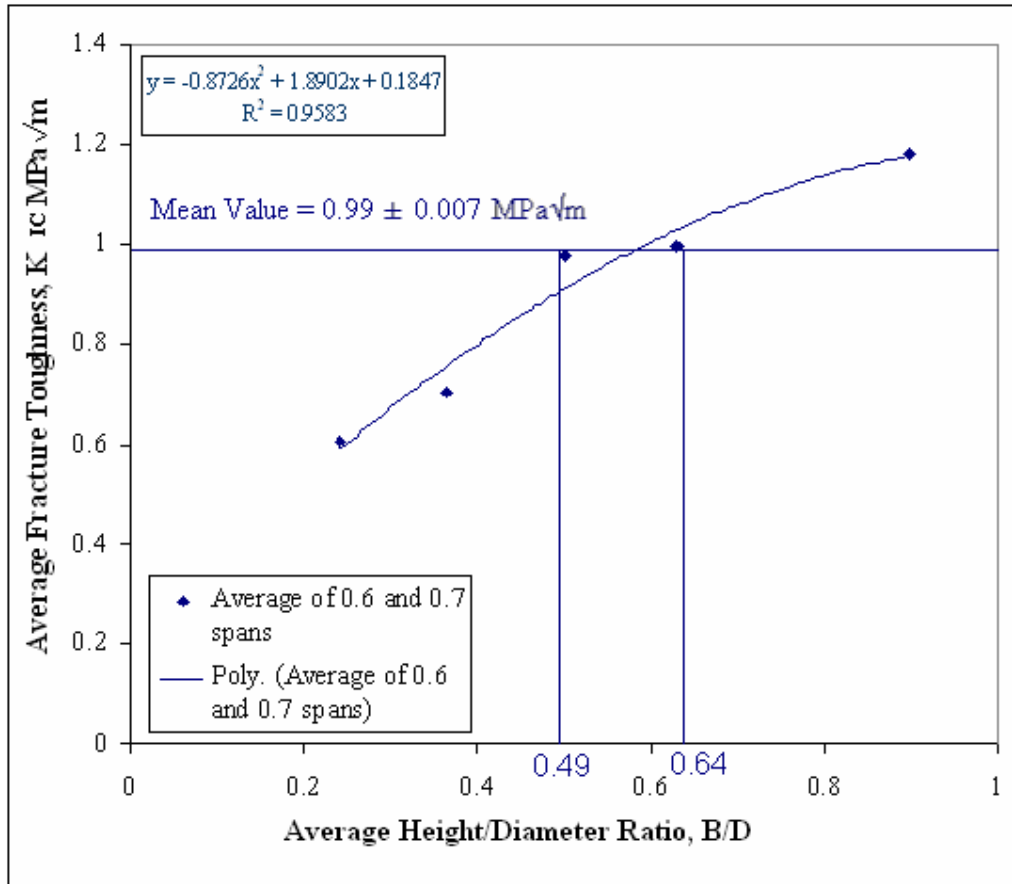


**Figure 6.9** Average fracture toughness versus average height/diameter ratio for all andesite specimens

#### 6.4 Results of Specimen Height Analysis for Marble

For marble SNDB specimens with a diameter of 75 mm and thicknesses between 22 – 54 mm were prepared. 1 to 4 tests were carried out for each group with 19 tests overall. S/R ratio was kept at 0.6. Results are given in table 6.3.

**Table 6.3** Results of S/R=0.6 marble specimens

Specimen Code	Failure Load $P_{CR}$ kN	SIF $K_I$ $Pa\sqrt{m}$	Normalized SIF $Y_I$	Fracture Toughness $K_{IC}$ $MPa\sqrt{m}$
Msndb2.2_06_1	1.44	286.29	2.87	0.413
Msndb2.2_06_2	1.38	302.34	2.96	0.418
Msndb3.2_06_1	3.89	150.09	1.89	0.585
Msndb3.2_06_2	4.01	123.09	1.67	0.493
Msndb4.0_06_1	6.39	102.20	1.63	0.626
Msndb4.2_06_1	8.72	78.03	1.31	0.681
Msndb4.2_06_2	8.35	69.91	1.28	0.584
Msndb4.2_06_3	8.61	68.01	1.26	0.586
Msndb4.5_06_1	10.14	68.01	1.23	0.636
Msndb4.5_06_2	11.97	69.12	1.33	0.827
Msndb4.5_06_3	12.67	64.28	1.25	0.815
Msndb4.5_06_4	9.07	62.95	1.17	0.571
Msndb4.7_06_1	9.32	60.14	1.15	0.561
Msndb4.7_06_2	12.92	58.17	1.17	0.751
Msndb4.7_06_3	13.91	58.17	1.17	0.809
Msndb5.0_07_1	15.39	51.62	1.106	0.794
Msndb5.0_07_2	16.49	51.62	1.102	0.851
Msndb5.4_06_1	19.56	46.89	1.072	0.917
Msndb5.4_06_2	17.36	46.89	1.067	0.813

The results are plotted as  $K_{IC}$  versus changing  $B/a$  in Figure 6.10 and changing  $B/D$  in Figure 6.11. The reason for generating two plots was that there were slight deviations in the specimen and notch dimensions for different specimens although the diameter was tried to be kept at 75 mm and notch length was tried to be kept around 10 mm. Again similar to the andesite case a better fit is obtained for plotting the results against  $B/D$  ratios, compared to the plots with  $B/a$  ratios.

It is seen from the behaviour in Figure 6.10 the increasing trend in fracture toughness with  $B/a$  diminishes above  $B/a$  values approximately around 4.0 to 5.1. If the fracture toughness values above  $B/a = 4.0$  is averaged fracture toughness value is found as  $0.72 \text{ MPa}\sqrt{\text{m}}$ . However,  $K_{IC}$  values for  $B/a$  between 4.0 and 5.1, don't seem to change much and they show a tendency to a constant value of  $0.70 \text{ MPa}\sqrt{\text{m}}$  when treated together, (Figure 6.10).

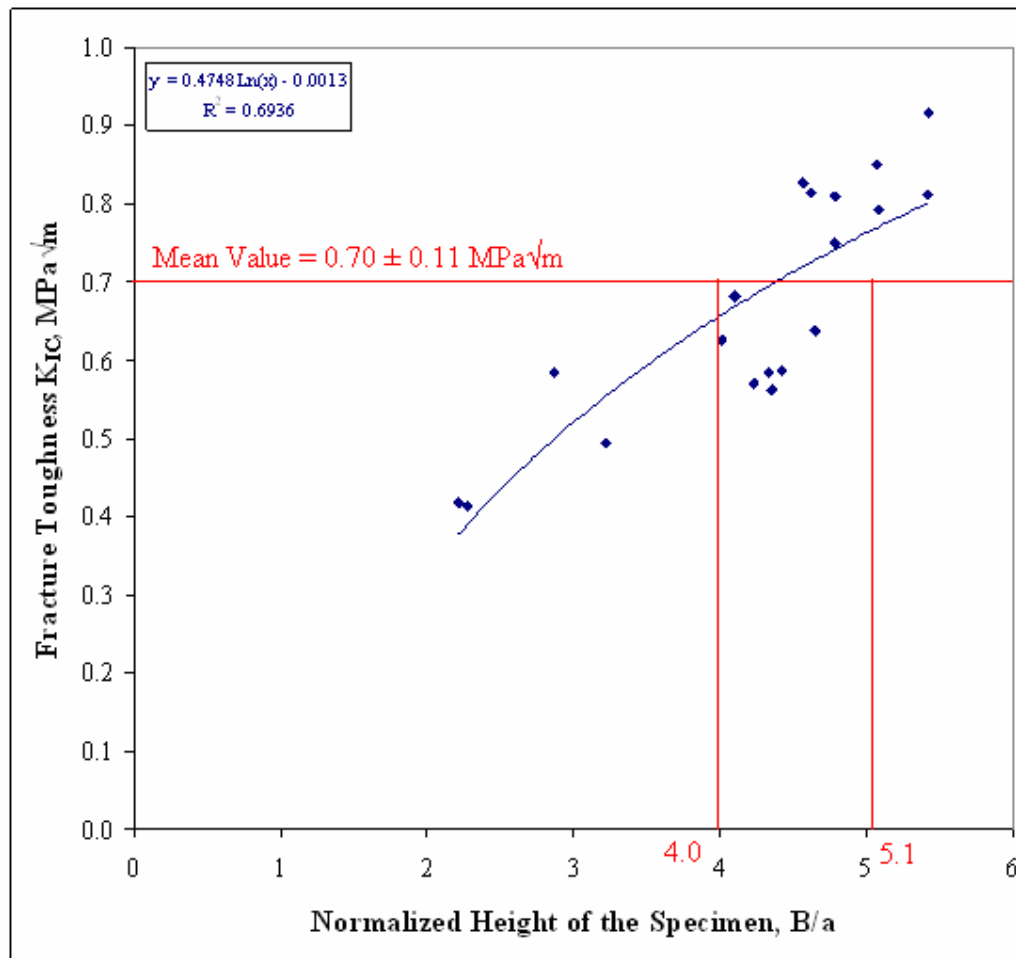


**Figure 6.10** Fracture toughness versus normalized height of the marble specimen, B/a

In Figure 6.11 if the fracture toughness values above  $B/D = 0.5$  is averaged fracture toughness value is found as  $0.72 \text{ MPa}\sqrt{\text{m}}$ . However,  $K_{IC}$  values for  $B/D$  between 0.5 and 0.7, dont seem to change much and they show a tendency to a constant value of  $0.70 \text{ MPa}\sqrt{\text{m}}$  when treated together, (Figure 6.11).

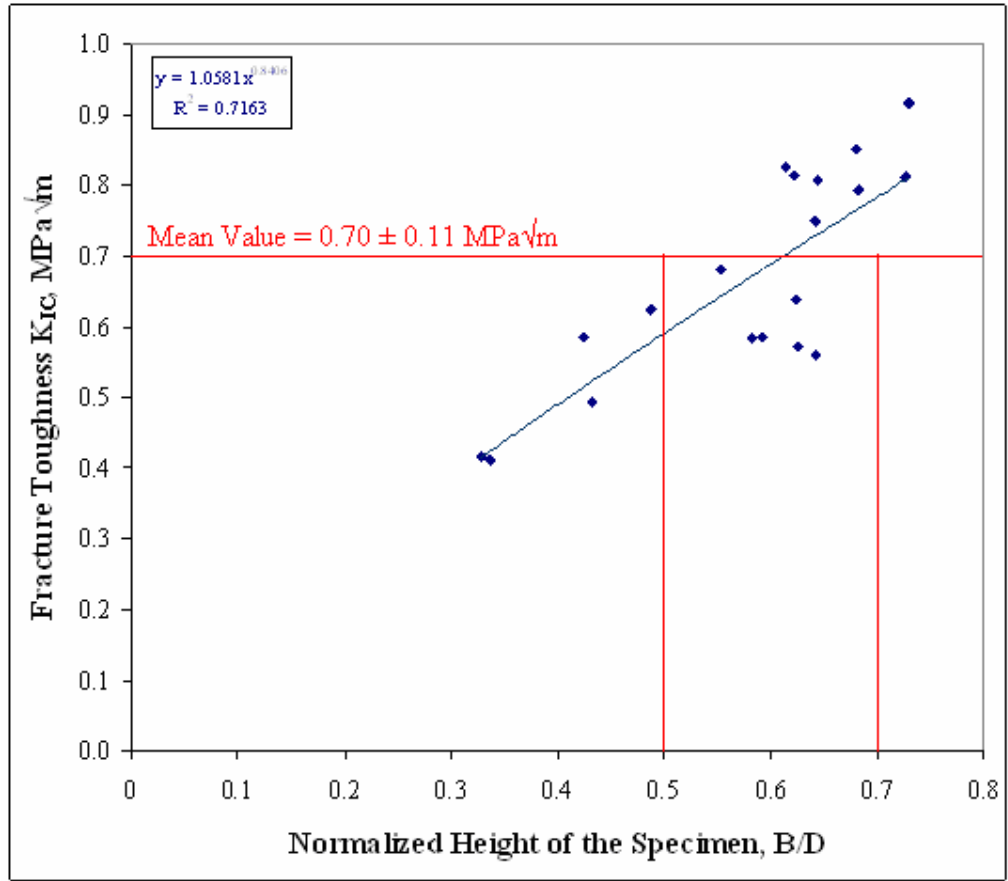


**Figure 6.11** Fracture toughness versus normalized height of the marble specimen, B/D

## 6.5 SCB Tests on Andesite and Marble

In order to compare the results of SNDB tests to a well-known test, SCB type specimens were prepared and tested for K<sub>IC</sub> determination for both andesite and marble rock types. The results are summarized in Table 6.4 for andesite and Table 6.5 for marble.

**Table 6.4** Results of marble SCB specimens

Specimen Code	Failure Load P <sub>CR</sub> kN	SIF K <sub>I</sub> $Pa\sqrt{m}$	Normalized SIF Y <sub>I</sub>	Fracture Toughness K <sub>IC</sub> $MPa\sqrt{m}$
Scb75_06_1	2.66	204.17	3.12	0.544
Scb75_06_2	2.98	204.17	3.16	0.609
Scb75_06_3	2.78	189.97	3.10	0.530
Scb75_06_4	2.41	189.97	3.07	0.459
Scb75_06_5	2.81	204.17	3.13	0.535
Average Fracture Toughness : $0.54 \pm 0.05 MPa\sqrt{m}$				

**Table 6.5** Results of andesite SCB specimens

Specimen Code	Failure Load P <sub>CR</sub> kN	SIF K <sub>I</sub> $Pa\sqrt{m}$	Normalized SIF Y <sub>I</sub>	Fracture Toughness K <sub>IC</sub> $MPa\sqrt{m}$
mScb75_06_1	3.87	206.57	3.14	0.799
mScb75_06_2	5.42	199.41	3.13	1.082
mScb75_06_3	4.13	211.75	3.24	0.874
mScb75_06_4	4.17	206.29	3.17	0.861
mScb75_06_5	4.68	190.19	3.04	0.889
Average Fracture Toughness : $0.90 \pm 0.1 MPa\sqrt{m}$				

By using these tables average fracture toughness value for marble from SCB tests are found as 0.54 MPa√m and for andesite 0.90 MPa√m. It should be noted in a previous study by Alıkkılıçgil (2006), fracture toughness value for Ankara Andesite is reported to be 0.93 MPa√m with SCB type specimens.

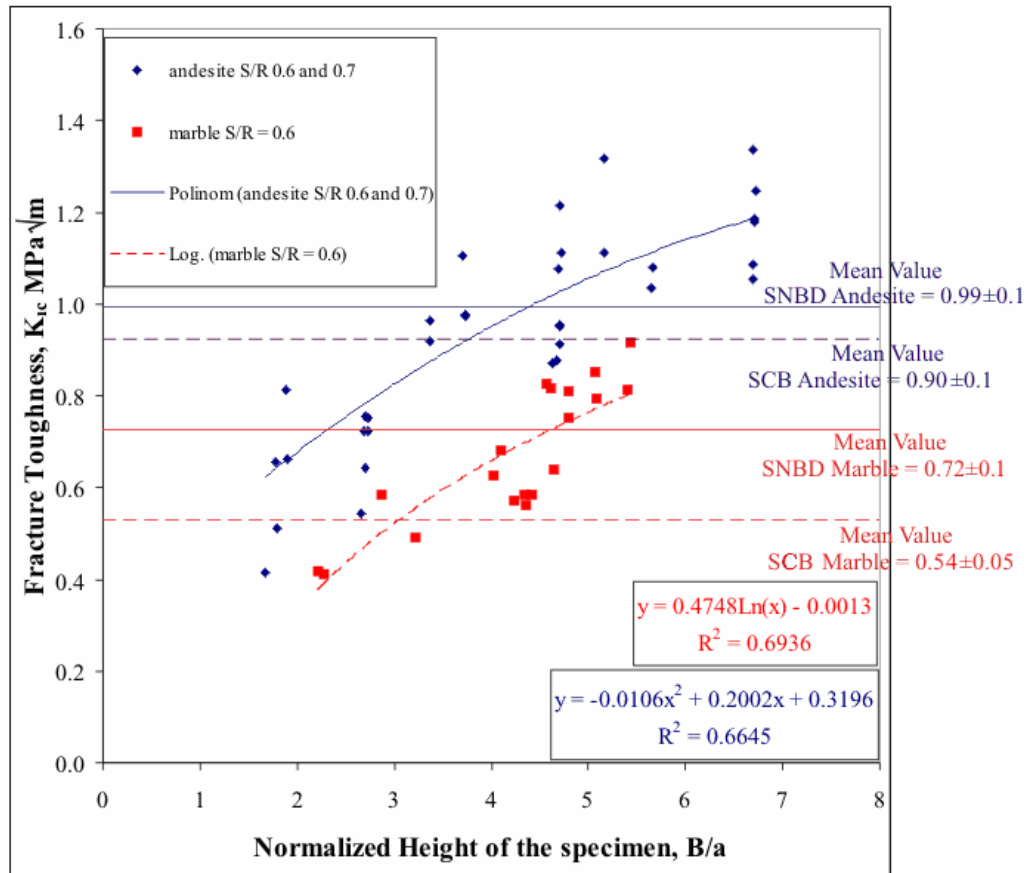


**Figure 6.12** Fracture toughness versus normalized height of the specimen

Considering the suggested testing height/notch length (B/A) limits, as seen from Figure 6.12 the SNDB average of andesite is 0.99 and SCB average is 0.90 so the SNDB value is %9 bigger than SCB value. For marble SNDB average is 0.72 and SCB average is 0.54 so SNDB value is %26 bigger than SCB value. Figure 6.12 shows that for marble quality of the fits is high and standard deviation for SCB tests is lower compared to the andesite. This is possibly due to the more homogeneous nature of the marble rock.

## 6.6 Stress Distributions Around the Notch Tip

In order to investigate the reason for having lower  $K_{IC}$  values for smaller specimen heights, stress distributions obtained from numerical models were studied. Stresses were found in MPa's at the point of crack propagation under the critical loads ( $P_{CR}$ ) for specimens with different specimen heights. This investigation was carried out for a typical andesite specimen with  $S/R = 0.6$ .

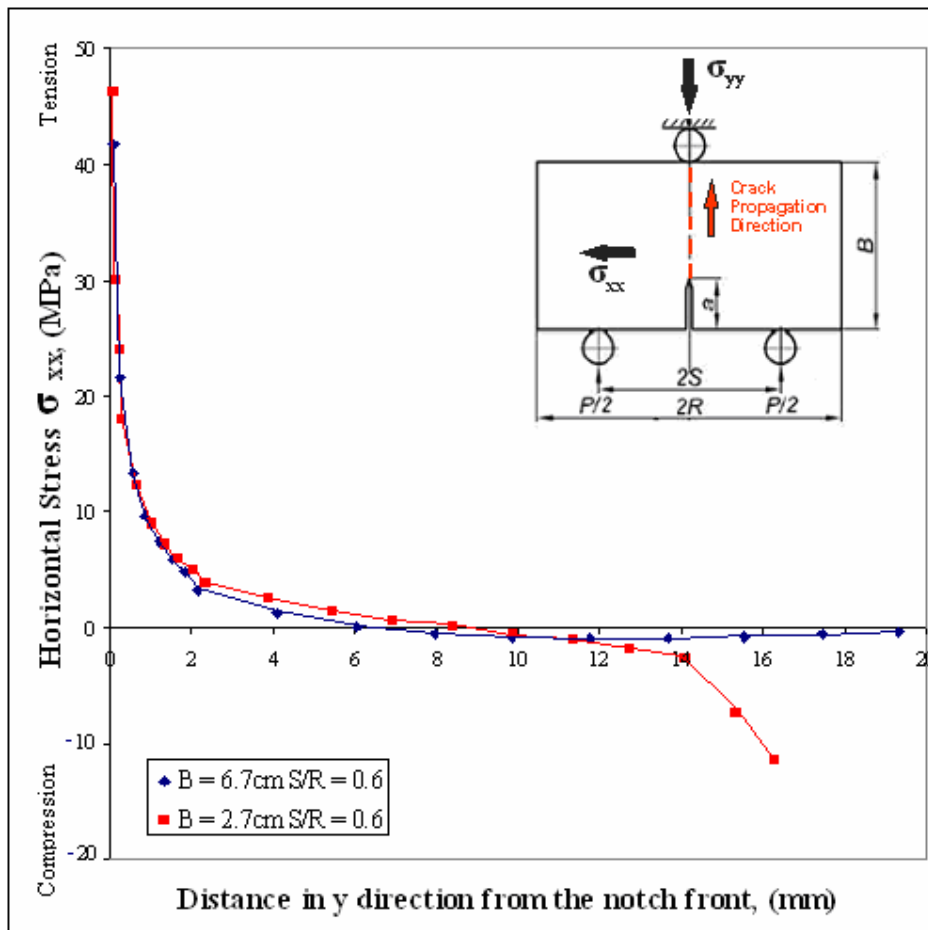


**Figure 6.13** Horizontal stress versus distance in y-direction from the notch front

Figure 6.13 shows the distribution of  $\sigma_{xx}$  stress component perpendicular to the notch plane. Figure 6.14 shows a detailed view of this distribution right at the notch tip where a crack is going to be initiated. For the smaller height case,  $\sigma_{xx}$  is about 20-100% higher in tension compared to the larger height specimen.

If a process or yield zone is going to develop due to the tensile stresses exceeding the tensile strength it is expected to be located within a couple of millimeters (1-5 mm) of the notch front with a comparable length to the initial notch of 10 mm length. So, a larger process zone is expected to develop in the smaller height specimen. Development of a process zone reduces the energy required to initiate and propagate the cracks and this means a lower  $K_{IC}$  is expected in this case, since  $K_{IC}$  and critical energy release rate  $G_C$  are directly related.

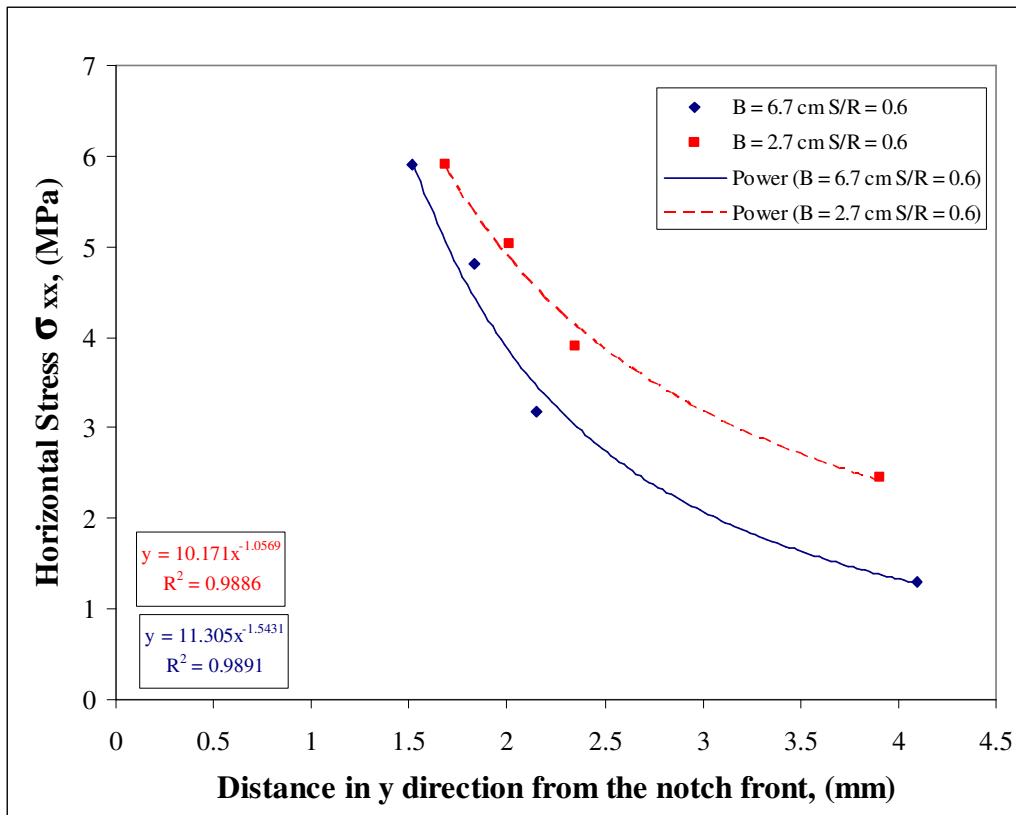


**Figure 6.14** Detailed view of horizontal stress versus distance in y-direction close to the notch front

Another reason for having larger  $K_{IC}$  values for thicker specimens can be explained by observing the stress distribution ( $\sigma_{yy}$ ) parallel to the crack front, Figure 6.15 shows the distribution of this stress along the vertical distance at the notch front. It is well known that crack planes in rock form perpendicular to the minimum principle stress ( $\sigma_3$ ) and crack propagation takes place parallel or in the direction of maximum principal stress ( $\sigma_1$ ). Maximum principal stress for the SNDB specimens is

compression and it occurs in y-direction under the roller support load at the upper boundary of the specimen. The higher this compression is the more well-defined crack propagation direction is obtained. As seen in Figure 6.15, for the smaller thickness specimen  $\sigma_{yy}$  turns to be compression about 2 mm earlier than the thicker specimen. This compression acts as the maximum principle stress  $\sigma_1$  and having the occurrence of  $\sigma_1$  closer to the notch front and having a higher compression here makes the crack forming from the notch finds its way easier for specimen with smaller heights or thicknesses.

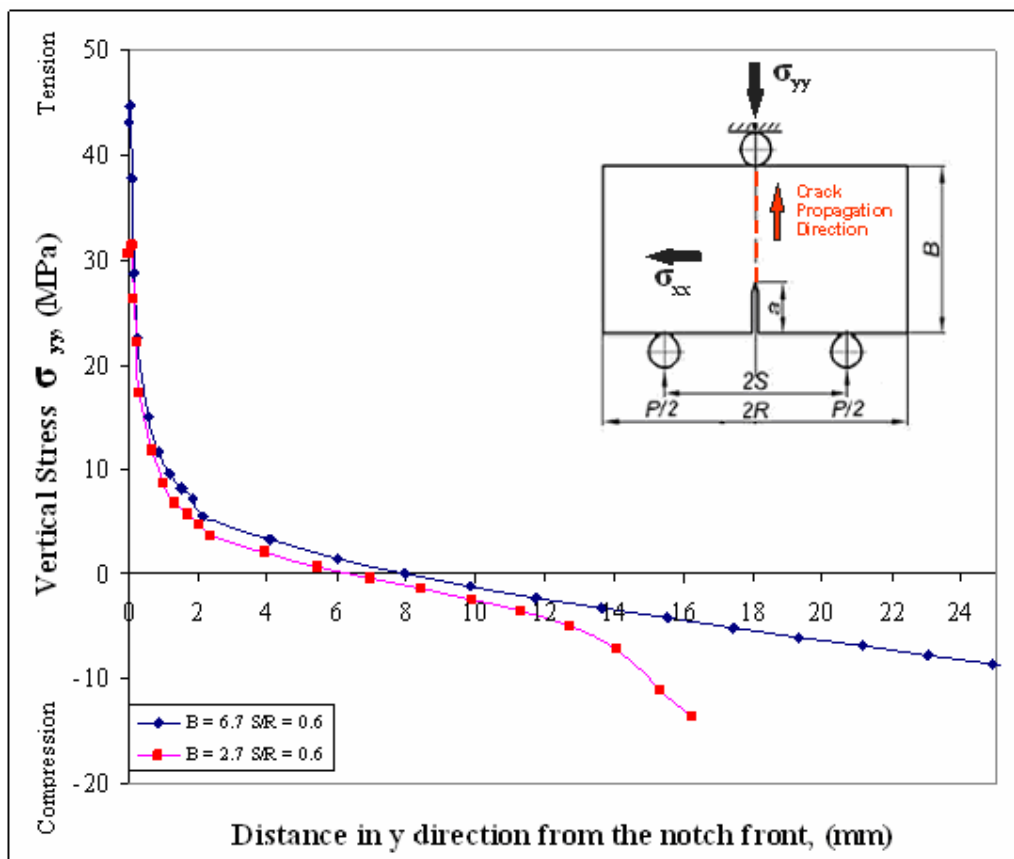


**Figure 6.15** Vertical stress versus distance in y-direction from the notch front

## CHAPTER 7

### CONCLUSION

New testing method Straight Notch Disc Bending (SNDB) was used for investigating specimen height effect on stress intensity factor and fracture toughness. Stress intensity factors were calculated by using 3D finite element program ABAQUS. Before the real modelling work verification of ABAQUS program was done by comparing the results of analysis to the analytical solutions of a well-known problem.

Changing span was found to have no significant effect on fracture toughness of Ankara Andesite, since the curves plotted to investigate this behaviour show no significant trends with changing S/R ratios.

In the numerical models it was found that stress intensity factor increases with the increasing specimen diameter for a fixed span/radius ratio. Stress intensity factor decreased with increasing specimen height (B) for SNDB type specimens.

Fracture toughness values were lower for specimens with smaller heights for both andesite and marble rock types. The suggested testing height interval for this type of specimens was found to be between height/diameter (B/D) ratios of 0.49 - 0.70, considering both andesite and marble rocks together. Similarly, suggested height/notch length (B/a) ratio was between 3.3-5.1 for both rocks.

Taking the averages for both tests staying within the limits above, fracture toughness values were determined as 0.99 for Ankara Andesite and 0.70 for Afyon Marble with SNDB method. These results were compared with results found from well-known semi-circular specimens under three-point bending (SCB). From SCB method fracture toughness values were found as 0.901 for andesite and 0.535 for marble.

Therefore, SCB tests produced lower values for fracture toughness of both rock types, compared to the values obtained by SNDB specimen geometry.

It was found that stress distributions around the notch tip were different for different specimen heights. For the smaller height specimen case, stress perpendicular to the notch plane was higher than the large thickness specimen around the notch front. Stress parallel to the crack plane turns to be compressive earlier along the crack front for the smaller height specimen. Also maximum principal stress or compression is higher for this case.

## **7.1 Recommendations**

In future work more rock types must be investigated with SNDB type and SCB type specimens in order to understand the mechanisms involved in having lower  $K_{IC}$  values with SCB technique.

Stress distributions for SCB and SNDB specimen geometries must be compared to understand the reason for having different  $K_{IC}$  values. This work is suggested to be carried out for the other specimen types such as Brazilian Disc fracture testing specimen geometries, Modified Ring fracture testing specimen geometries and the others.

## REFERENCES

ABAQUS/CAE User's Manual, Version 6.5 Documentation.

Alber, M., "Factors influencing fracture toughness  $K_{IC}$  from simple screening tests", Int. J. of Rock Mech. Min. Sciences, Technical Note, Vol. 40, pp. 779-784, 2003.

Alkılıçgil, Ç., "Development of New Method for Mode I Fracture Toughness Test on Disc Type Rock Specimens" M.S. Thesis, METU, Ankara, 145 p., 2006.

Al-Shayea, N., "Comparing Reservoir and Outcrop Specimens for Mixed Mode I-II Fracture Toughness of a Limestone Rock Formation at Various Conditions", Rock Mech. Rock Engng., Vol. 35, Issue 4, pp. 271-297, 2002.

Anderson, T.L., "Fracture mechanics: Fundamentals and Applications", CRC Press, Inc., Florida, 1991.

Atkinson, B.K., "Subcritical crack growth in geological materials". J. Geophys. Res.; 89: 4077-4114, 1984.

Atkinson, B.K., "Fracture Mechanics of Rock", Academic Press, London, 1987.

Ayatollahi, M.R and Aliha, M.R.M., "On determination of mode II fracture toughness using semi-circular bend specimen", International Journal of Solids and Structures, Volume 43, Issue 17 , pp. 5217-5227, August 2006.

Ayatollahi, M.R and Aliha, M.R.M., "Wide range data for crack tip parameters in two disc-type specimens under mixed mode loading", Computational Materials Science, Artical in Press, 2006.

Backers, T., et al, "Effect of loading rate on Mode I fracture toughness, roughness and micromechanics of sandstone", Int. J. of Rock Mech. Min. Sci., Technical Note, Vol. 40, pp. 425-433, 2003.

Backers, T., et al. ," New data on mode II fracture toughness of rock from the punch-through shear test", Int. J. of Rock Mech. Min. Sci., Vol. 41, Paper 1A 01, 2004.

Balme, M.R., "Fracture toughness measurements on igneous rocks using a highpressure, high- temperature rock fracture mechanics cell", Journal of Volcanology and Geothermal Research, Vol. 132, pp.159-172,2004.

Basbay, O., "Investigation of Mixed Mode Crack Propagation from Preexisting Notches in Brazilian Discs of Ankara Andesite", M.S. Thesis, METU, Ankara, 168 p., 2002.

Bearman, R.A., "The use of the point load test for the rapid estimation of Mode I fracture toughness", *Int. J. Rock Mech. Min. Sci.*, Vol. 36, pp. 257-263, 1999.

Chang, J., "A General Mixed-Mode Brittle Fracture Criterion for Cracked Materials", *Engineering Fracture Mechanics*, Vol. 73, 1249-1263, 2006.

Chang, S. H., Chung-In Lee, Jeon, S., "Measurement of rock fracture toughness under modes I and II and mixed-mode conditions by using disc-type specimens", *Engineering Geology*, Vol. 66, pp. 79-97, 2002.

Chong, K.P. & Kuruppu, M.D. "New specimen for fracture toughness determination of rock and other materials", *Int. J. Fract.*; 26: 59-62, 1984.

Chong, K.P. and Kuruppu, M.D., "New specimens for mixed mode fracture investigations of geomaterials", *Engineering Fracture Mechanics*, Vol. 30, no. 5, p. 701-712, 1988.

DaqView and DaqViewXL Documents.

Fowell, R. J. and Chen, J. F., "The third chevron-notch rock fracture specimen-the cracked chevron-notched Brazilian disk". *Proc. 31st U.S. Symp. on Rock Mechanics*, pp. 295-302, 1990.

ISRM Commission on Standardization of Laboratory and Field Tests, "Suggested Methods for Determining Tensile Strength of Rock Materials", *Int. J. Rock Mech. Min. Sci. & Geomech. Abstr.*, Vol. 15, pp. 99-103, 1978.

ISRM Commission on Standardization of Laboratory and Field Tests, "Suggested Methods for Determining the Uniaxial Compressive Strength and Deformability of Rock Materials", *Int. J. Rock Mech. Min. Sci. & Geomech. Abstr.*, Vol. 16, pp. 135-140, 1979.

Irwin, G.R., "Fracture. In: *Handbuch der Physik.*", Springer Verlag, Berlin, Vol. 6, 1958.

Irwin, G.R., "Fracture Dynamics." *Fracturing of Metals*, American Society for metals, Cleveland, pp. 147-166, 1948.

Irwin, G.R., "Onset of Fast Crack Propagation in High Strength Steel and Aluminum Alloys." *Sagamore Research Conference Proceedings*, Vol.2, pp.289-305, 1956.

Irwin, G.R., "Plastic Zone Near a Crack and Fracture Toughness." *Sagamore Research Conference Proceedings*, Vol. 4, 1961.

ISRM Commission on Testing Methods, "Suggested Method for Determining Fracture Toughness of Rocks", *Int. J. Rock Mech. Min. Sci. & Geomech. Abstr.*, Vol. 25, pp. 71-96, 1988.

ISRM Commission on Testing Methods, "Suggested Method for Determining Mode I Fracture Toughness Using Cracked Chevron Notched Brazilian Disc (CCNBD) Specimens", *Int. J. Rock Mech. Min. Sci. & Geomech. Abstr.*, Vol. 32, pp. 57-64, 1995.

Janssen M., J. Zuidema, R.J.H. Wanhill Sun, G., "Fracture Mechanics", Elsevier, New York, 2002.

Khan, K. and Al-Shayea, N. A., "Effect of Specimen Geometry and Testing Method on Mixed Mode I-II Fracture Toughness of a Limestone Rock from Saudi Arabia", *Rock Mech. Rock Engng.*, Vol. 33, pp. 179-206, 2000.

Lim, I.L., Johnston, I.W., Choi, S.K. and Boland, J.N., "Fracture Testing of a Soft Rock with Semi-circular Specimens Under Three-point Bending. Part I-Mode I", *Int. J. Rock Mech. Min. Sci. & Geomech. Abstr.*, Vol. 31, No. 3, pp. 185-197, 1994.

Lim, I.L., Johnston, I.W., Choi, S.K. and Boland, J.N., "Fracture Testing of a Soft Rock with Semi-circular Specimens Under Three-point Bending. Part II- Mixed Mode", *Int. J. Rock Mech. Min. Sci. & Geomech. Abstr.*, Vol. 31, No. 3, pp. 199-212, 1994.

Lim, I.L., et.al, "Stress intensity factors for semi-circular specimens under threepoint bending", *Engineering Fracture Mechanics*, Vol. 44, No. 3, pp. 363-382, 1993.

Matsuki, K., Nozuyama, Y. and Takahashi, H., "Size effect in the fracture toughness testing of rocks using a boring core", *Proc. Spring Meeting Min. Metall. Inst, Japan*, pp. 193-194, 1987.

M.R. Ayatollahi , M.R.M. Aliha., "Wide range data for crack tip parameters in two disc-type specimens under mixed mode loading" *Fatigue and Fracture Laboratory, Department of Mechanical Engineering, Iran University of Science and Technology, Narmak, Tehran 16844, Iran, pp 661-669 2006*

MTS System Catalog, 1992.

Nordlund, E., Li, C., Carlsson, B., "Mechanical properties of the diorite in the prototype repository at Äspö HRL—laboratory tests", *International Progress Report, IPR-99-25, SKB, June 1999.*

Ouchterlony, F., "A presentation of the ISRM Suggested Methods for determining fracture toughness of rock material", *Proc. 6th Int. Congr. Rock Mechanics, Balkema, Rotterdam, Vol. 2, pp. 1181-1186, 1987.*

Ouchterlony, F., "Suggested methods for determining the fracture toughness of rock", *Int. J. Rock Mech Min. Sci., ISRM Working Group Report, Vol. 25, pp 71-96, 1988.*

Rossmann H. P. "Rock Fracture Mechanics", CISM, Udine , 1983

Shi, X.Q., "Determination of interface fracture toughness of adhesive joint subjected to mixed-mode loading using finite element method", *International Journal of Adhesion & Adhesives*, Vol. 26, pp. 249-260, 2006.

Sousa, J.L.A.O. and Bittencourt, T.N., "Experimental Analysis of Fracture Processes in Concrete", *Journal of the Brazilian Society of Mechanical Sciences*, Vol. 23, No. 4, 2001.

Soo-Ho Chang, Chung-In Lee, Seokwon Jeon, "Measurement of rock fracture toughness under modes I and II and mixed-mode conditions by using disc-type specimens", School of Civil, Urban and Geosystem Engineering, Seoul National University, Seoul, South Korea, pp. 79-97, 2002

Sener, S., "Fracture Toughness Tests on Brazilian Discs of Ankara Andesite", M.S. Thesis, METU, Ankara, 122 p., 2002.

Wang, Q.Z., "Stress Intensity Factors of the ISRM Suggested CCNBD Specimen Used for Mode-I Fracture Toughness Determination", *Int. J. of Rock Mech. Min. Sci.*, Vol. 35, No. 7, pp. 977-982, 1998.

Whittaker, B.N., Singh, R.N., Sun, G., "Rock Fracture Mechanics-Principles, Design and Applications", Elsevier, Amsterdam, 1992.

Yoon, J. and Jeon, S., "Experimental verification of a PTS mode II test for rock", *Int. J. of Rock Mech. Min. Sci.*, Vol. 41, Paper 1A 02, 2004.

Zafošnik, B., "Evaluation of stress intensity factors using finite elements", Laboratory for Computer Aided Engineering, Faculty of Mechanical Engineering, University of Maribor, Maribor, Slovenija, 2000.

Zhang, Z.X., "An empirical relation between mode I fracture toughness and the tensile strength of rock", *Int. J. of Rock Mech. Min. Sci.*, Technical Note, Vol. 39, pp. 401-406, 2002.

# APPENDIX A

## SPECIMEN DIMENSIONS TABLES

### A.1 Specimen Height Effect on Fracture Toughness Analysis for Andesite

**Table A.1** Average dimensions of S/R=0.6 andesite SNDB specimens

Specimen Code	a (mm)	D (mm)	R (mm)	B (mm)	S (mm)	B/a	B/D	S/R
sndb037_06	10.00	74.84	37.42	27.13	22.45	2.71	0.31	0.6
sndb027_06	10.00	74.68	37.34	37.07	22.41	3.37	0.50	0.6
sndb021_06	10.00	74.95	37.47	47.07	22.49	4.71	0.63	0.6
sndb015_06	10.00	74.76	37.38	67.11	22.43	6.71	0.90	0.6

**Table A.2** Average dimensions of S/R=0.7 andesite SNDB specimens

Specimen Code	a (mm)	D (mm)	R (mm)	B (mm)	S (mm)	B/a	B/D	S/R
sndb037_07	10.00	74.23	37.11	26.95	25.98	2.70	0.36	0.7
sndb027_07	10.00	73.98	36.99	37.19	25.90	3.72	0.50	0.7
sndb021_07	10.00	73.97	36.98	46.75	25.89	4.68	0.63	0.7
sndb015_07	10.00	74.58	37.29	67.06	26.11	6.71	0.90	0.7

**Table A.3** Average dimensions of S/R=0.8 andesite SNDB specimens

Specimen Code	a (mm)	D (mm)	R (mm)	B (mm)	S (mm)	B/a	B/D	S/R
sndb037_08	10.87	75.00	37.50	26.85	30.00	2.47	0.36	0.8
sndb027_08	10.50	75.00	37.50	36.84	30.00	3.51	0.49	0.8
sndb021_08	10.75	75.00	37.50	46.98	30.00	4.37	0.63	0.8
sndb015_08	10.75	74.99	37.49	66.74	29.99	6.21	0.90	0.8

**Table A.4** Average dimensions of  $S/R=0.9$  andesite SNDB specimens

Specimen Code	a (mm)	D (mm)	R (mm)	B (mm)	S (mm)	B/a	B/D	S/R
sndb037_09	10.87	74.87	37.43	26.92	33.69	2.48	0.36	0.9
sndb027_09	10.25	75.02	37.51	36.93	33.76	3.60	0.49	0.9
sndb021_09	10.63	75.03	37.51	46.92	33.76	4.41	0.63	0.9

## A.2 Specimen Height Effect on Fracture Toughness Analysis for Marble

**Table A.5** Dimensions of S/R=0.6 marble SNDB specimens

Specimen Code	a (mm)	D (mm)	R (mm)	B (mm)	S (mm)	B/a	B/D	S/R
msndb25_06_1	11	74.45	37.23	25.08	22.34	2.28	0.34	0.6
msndb25_06_2	11	74.44	37.22	24.42	22.33	2.22	0.33	0.6
msndb32_06_1	10	74.47	37.24	32.36	22.34	3.24	0.43	0.6
msndb32_06_2	11	74.47	37.23	31.58	22.34	2.87	0.42	0.6
msndb32_06_3	10	74.51	37.26	32.17	22.35	3.20	0.43	0.6
msndb36_06_1	9	74.05	37.03	36.15	22.22	4.02	0.49	0.6
msndb41_06_1	10	74.17	37.09	41.01	22.25	4.10	0.55	0.6
msndb43.4_06_1	10	74.36	37.18	43.37	22.31	4.34	0.58	0.6
msndb44.4_06_1	10	74.54	37.27	44.15	22.36	4.42	0.59	0.6
msndb45_06_1	10	74.37	37.18	45.68	22.31	4.57	0.61	0.6
msndb46_06_1	10	74.22	37.11	46.18	22.27	4.62	0.62	0.6
msndb46_06_2	11	74.44	37.22	46.63	22.33	4.24	0.63	0.6
msndb46_06_3	10	74.54	37.27	46.51	22.36	4.65	0.62	0.6
msndb48_06_1	11	74.54	37.27	47.89	22.36	4.35	0.64	0.6
msndb48_06_2	10	74.58	37.29	47.85	22.37	4.79	0.64	0.6
msndb48_06_3	10	74.48	37.24	47.87	22.34	4.79	0.64	0.6
msndb50_06_1	10	74.58	37.29	50.87	22.37	5.09	0.68	0.6
msndb50_06_2	10	74.48	37.24	50.72	22.34	5.07	0.68	0.6
msndb54_06_1	10	74.50	37.25	54.33	22.35	5.43	0.73	0.6
msndb54_06_2	10	74.38	37.19	54.08	22.31	5.41	0.73	0.6

### A.3 SCB Specimens for Comparing Results

**Table A.6** Dimensions of andesite SCB Specimens

Specimen Code	a (mm)	D (mm)	R (mm)	B (mm)	S (mm)	B/a	S/R
scb_1	10	74.54	37.27	36.62	22.36	3.66	0.6
scb_2	10	75.14	37.57	37.31	22.54	3.73	0.6
scb_3	10	75.05	37.53	36.18	22.52	3.62	0.6
Scb_4	10	75.11	37.56	36.74	22.53	3.67	0.6
scb_5	10	75.10	37.55	37.89	22.53	3.79	0.6

**Table A.7** Dimensions of marble SCB Specimens

Specimen Code	a (mm)	D (mm)	R (mm)	B (mm)	S (mm)	B/a	S/R
mscb_1	10	74.55	37.28	36.56	22.37	3.66	0.6
mscb_2	10	74.60	37.30	36.96	22.38	3.70	0.6
mscb_3	9	74.61	37.31	37.08	22.38	3.71	0.6
mscb_4	9	74.57	37.29	36.63	22.37	3.66	0.6
mscb_5	10	74.60	37.30	37.02	22.38	3.70	0.6

## APPENDIX B

### SPECIMEN FRACTURE TOUGHNESS RESULTS TABLES

#### B.1 All Specimen Results of Fracture Toughness For Andesite

**Table B.1** Results of S/R=0.8 andesite specimens

Specimen Code	P <sub>CR</sub> kN	K <sub>I</sub> $Pa\sqrt{m}$	Y <sub>I</sub>	K <sub>IC</sub> (Fracture Toughness) $MPa\sqrt{m}$
Sndb2.7_08_1	2.37	320.34	3.487	0.765
Sndb2.7_08_2	2.84	320.34	3.487	0.916
Sndb2.7_08_3	2.44	320.34	3.487	0.786
Sndb2.7_08_4	2.41	320.34	3.487	0.756
Sndb3.7_08_1	6.81	142.34	2.161	0.964
Sndb3.7_08_2	7.25	142.34	2.161	1.031
Sndb3.7_08_3	6.79	142.34	2.161	0.989
Sndb3.7_08_4	5.10	142.34	2.161	0.709
Sndb4.7_08_1	12.00	89.49	1.714	1.063
Sndb4.7_08_2	12.60	89.49	1.714	1.138
Sndb4.7_08_3	12.00	89.49	1.714	1.084

**Table B.2** Results of S/R=0.9 andesite specimens

Specimen Code	P <sub>CR</sub> kN	K <sub>I</sub> $Pa\sqrt{m}$	Y <sub>I</sub>	K <sub>IC</sub> (Fracture Toughness) $MPa\sqrt{m}$
Sndb2.7_09_1	1.98	357.861	3.899	0.724
Sndb2.7_09_2	2.27	357.861	3.899	0.785
Sndb3.7_09_1	6.27	159.845	2.474	1.017
Sndb3.7_09_2	5.68	159.845	2.474	0.898
Sndb3.7_09_3	6.06	159.845	2.474	0.986
Sndb3.7_09_4	5.84	159.845	2.474	0.923
Sndb4.7_09_1	12.3	102.358	1.969	1.213
Sndb4.7_09_2	12.00	102.358	1.969	1.249
Sndb4.7_09_3	12.40	102.358	1.969	1.295

**B.2 Average Results of Fracture Toughness For Andesite****Table B.3** Results of S/R=0.6 andesite specimens (Average Values)

Specimen Code	P <sub>CR</sub> kN	K <sub>I</sub> $Pa\sqrt{m}$	Y <sub>I</sub>	K <sub>IC</sub> (Fracture Toughness) $MPa\sqrt{m}$
Sndb2.7_06	4.20	210.70	2.417	0.883
Sndb3.7_06	9.81	109.05	1.623	1.070
Sndb4.7_06	17.13	63.63	1.268	1.094
Sndb6.7_06	32.83	35.74	1.013	1.174

**Table B.4** Results of S/R=0.7 andesite specimens (Average Values)

Specimen Code	P <sub>CR</sub> kN	K <sub>I</sub> $Pa\sqrt{m}$	Y <sub>I</sub>	K <sub>IC</sub> (Fracture Toughness) $MPa\sqrt{m}$
Sndb2.7_07	2.65	251.67	2.844	0.666
Sndb3.7_07	8.18	124.75	1.939	1.020
Sndb4.7_07	12.73	70.94	1.385	0.902
Sndb6.7_07	25.90	48.59	1.373	1.259

**Table B.5** Results of S/R=0.8 andesite specimens (Average Values)

Specimen Code	P <sub>CR</sub> kN	K <sub>I</sub> $Pa\sqrt{m}$	Y <sub>I</sub>	K <sub>IC</sub> (Fracture Toughness) $MPa\sqrt{m}$
Sndb2.7_08	2.52	320.34	3.487	0.806
Sndb3.7_08	6.49	142.35	2.161	0.923
Sndb4.7_08	12.20	89.50	1.714	1.092

**Table B.6** Results of S/R=0.9 andesite specimens (Average Values)

Specimen Code	P <sub>CR</sub> kN	K <sub>I</sub> $Pa\sqrt{m}$	Y <sub>I</sub>	K <sub>IC</sub> (Fracture Toughness) $MPa\sqrt{m}$
Sndb2.7_09	2.36	357.86	3.899	0.843
Sndb3.7_09	5.96	159.85	2.474	0.953
Sndb4.7_09	12.23	102.36	1.969	1.252

# APPENDIX C

## SPECIMEN PHOTOS AFTER EXPERIMENTS

### C.1 SNDB Ankara Andesite Specimens Photos After Experiments



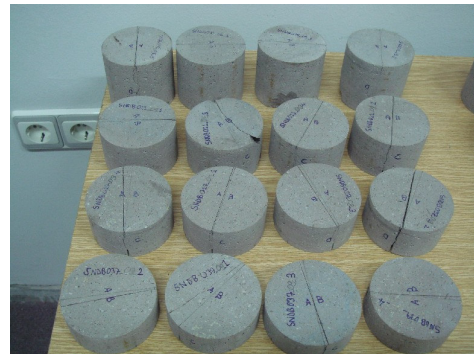
(a)  $S/R = 0.6$



(b)  $S/R = 0.7$



(c)  $S/R = 0.8$



(d)  $S/R = 0.9$

**Figure C.1** Andesite SNDB specimens after experiments according to  $S/R$

### C.2 SNDB Afyon Marble Specimens Photos After Experiments



**Figure C.2** Marble SNDB specimens after experiments

### C.3 SCB Specimens Photos After Experiments



**Figure C.3** Andesite and marble SCB specimens after experiments